2017

ELECTRO-OPTIC CONTACT POLING OF POLYMER WAVEGUIDE DEVICES AND THIN FILMS

Michael Briseno
Michigan Technological University, mjbrisen@mtu.edu

ELECTRO-OPTIC CONTACT POLING OF POLYMER WAVEGUIDE DEVICES AND THIN FILMS

By

Michael Joseph Briseno

A THESIS

Submitted in partial fulfillment of the requirements for the degree of

MASTER OF SCIENCE

In Electrical Engineering

MICHIGAN TECHNOLOGICAL UNIVERSITY

2017

This thesis has been approved in partial fulfillment of the requirements for the Degree of MASTER OF SCIENCE in Electrical Engineering.

Department of Electrical and Computer Engineering

Thesis Advisor:	*Dr. Christopher T. Middlebrook*
Committee Member:	*Dr. Durdu Guney*
Committee Member:	*Dr. Elena Semouchkina*
Committee Member:	*Dr. Miguel Levy*
Department Chair:	*Dr. Daniel R. Fuhrmann*

Dedication

It took 2 years to complete this degree. Even though I know most of you won't read this, I would like to dedicate this work to those of whom who pressured me into taking time to relax and enjoy life during college. If we go by number of beers (which I believe is the best parameter), Jack is the overwhelming winner and I thank him for the countless stories we made.

Runner ups in no particular order: Donald, Taylor, Nick, Ekramul, and Rachel.

Also shout out to 1001 (Starting from the penthouse: John, Martin, Matt, Adam, Kris, and Kyle) for an unforgettable undergraduate career.

Contents

List of Figures

List of Tables

Preface

This thesis is ultimately based on the fabrication and experimental work of internal research done within our group at Michigan Technological University. My advisor Dr. Christopher Middlebrook and researchers Arash Hosseinzadeh, Mashad Uddin Saleh, Derek Burrell, and Evan Gawron. None of the text of the thesis is taken directly from previously published or collaborative articles.

The electro-optic poling setup and two-tone test/coupling bench was constructed primarily myself with input from the group. The initial characterization for fabrication of thin films and devices was done in large part by Arash, Mashad, and Dr. Middlbrook. Partial work done by Evan and myself. The data collection and analysis are my original work.

Acknowledgments

I would like to thank all those who have helped me learn, understand, and appreciate the field of optics and photonics. Many individuals have allowed me to be successful in my research endeavors during my Master's degree.

I would first like to thank my group for advising and fostering my learning by being open to questions/discussion and sharing the excitement of our field of study: Arash Hosseinzadeh, Mashad Uddin Saleh, Derek Burrell, Evan Gawron, and Dr. Kevin Kruse. In addition, the support of Dolendra Karki, Ashim Chakravarty, Wyatt Adams, and Dr. Jason Sommerville for taking time to assist me with experimental setup and measurements.

Additionally, ECE department staff for guiding my through any questions I had about forms and deadlines. They really allow this department function smoothly: Joan Becker, Lisa Hitch, and Michele Kamppinen. Also, Mark Sloat, Chuck Sannes, and John Kolacz for being wizards in rigging up solutions to any problem I came to them with. In addition Dr. Glen Archer for working with me in Circuits, Intro to C, Laser, and Photonic Materials labs while I was in my graduate teaching assistant role.

A large portion of the fabrication work was done in the Microfabrication Facility and

I would like to thank the facility along with Dr. Chito Kendrick for all the advice and availability during fabrication.

DARPA and NAVSEA Crane for funding projects intertwined in the work for this thesis. Jingdong Lou at Soluxra for his valuable insight into working with SEO100C.

My defense committee for their time reviewing this thesis: Dr. Durdu Guney, Dr. Elena Semouchkina, and Dr. Miguel Levy.

Lastly and probably the most I would like to thank Dr. Christopher Middlebrook for believing in me. It took a lot of effort on his part to convince me to pursue a MS degree. The unfaltering confidence and trust he had in me allowed intellectual growth. He always says, "You can't make diamonds without pressure."

List of Abbreviations

A	Area
APC	Angled Polished Connector
CF_4	Carbon Tetrafluoride
d	Film Thickness
DFB	Distributed Feedback
DR-1	Disperse Red-1 Chromophore
E	Electric Field
EO	Electro-Optic
f	Frequency
FC	Physical Connection
FR4	Flame Retardant 4 Glass Reinforced Epoxy Laminate Sheet
Γ	Overlap Integral
I	Current
IMD	Intermodulation Distortion
ITO	Indium Tin Oxide
IR	Infrared
I-V	Current-Voltage
L	Length

λ	Wavelength
$LiNbO_3$	Lithium Niobate
MZI	Mach-Zehnder Interferometer
n	Refractive Index
N_2	Nitrogen Gas
NOA73	Northland Optical Adhesives 73
NR9-1500P	Negative Photoresist 1500 Series
O_2	Di-Oxygen
PMMA	Poly(methyl methacrylate)
PR1-1000	Positive Photoresist 1000 Series
ρ	Resistivity
R	Resistance
RCA	Radio Company of America
RF	Radio Frequency
RIE	Reactive Ion Etch
R_a	Average Roughness
R_q	Root-Mean Square Roughness
r_{33}	Electro-Optic Coefficient
r_{13}	Electro-Optic Coefficient
RD6	Resist Developer Number 6
SEO100C	Soluxra Electro-Optic 100C Formulation

SEO125B	Soluxra Electro-Optic 125B Formulation
SMA	SubMiniature version A
T_g	Glass Transition Temperature
TIR	Total Internal Reflection
UV	Ultra-Violet
UV15LV	Ultra-Violet Epoxy Low Viscosity
V	Voltage
VI	Virtual Instrument File

Abstract

Optical communication is a high speed, large bandwidth, low cost, and power efficient method of transferring data over short-haul and long-haul channels. Optical communication requires devices (optical modulators) that utilize the originating electrical signal information to modulate a corresponding optical signal. State of the art optical modulators can be used for communicating signals at modulation frequencies up to 100 GHz and faster. Polymer modulators are used over lithium niobate due to the large potential electro-optic coefficient, which has been shown to be as high as 226 pm/V in thin films.

Organic electro-optic polymers used in thin film modulators contain nonlinear optical chromophore dipoles that when aligned produce an electro-optic coefficient from the pockels effect. The magnitude of the electro-optic coefficient is dependent on the strength and uniformity of the electric field applied to the thin film polymer. In multi-layer devices the applied field is determined by design, fabrication, layer thickness, and pinhole defects that cause dielectric breakdown of the device. A laboratory process was designed and created for electro-optic contact poling of waveguide devices and thin film polymers. A sample is heated to the glass transition temperature of the electro-optic polymer and an electric field is applied to allow alignment

of chromophores. The sample is then cooled to room temperature to lock the chromophores in place. Soluxra SEO100C polymer is used for validation of the poling process because of its high electro-optic coefficient potential.

First time large area contact poling of electro-optic polymer thin films is performed and verified enabling the use of electro-optic polymers in a variety of applications. The index of refraction change after poling was measured in Soluxra SEO100C spun thin films using a prism coupler to verify poling. TM index of refraction of thin film SEO100C increased by 0.00402-0.00486 with voltages of 39-51 V/μm after poling. SEO100C thin films were exposed to processing steps used during fabrication of devices for proof of concept for electro-optic poling mid-process in reduce applied voltage. The TM indexes relaxed an average of 16% back to their original values when exposed to the extra processing. A laboratory was built for electro-optic coefficient and performance calculation in multi-layer devices for future verification of poling. The half-wave voltage (V_π) and intermodulation distortion (IMD) was shown as a proof-of-concept on a commercial Mach-Zehnder modulator.

Chapter 1

Introduction

Optical communication links offer lower cost, lower power attenuation, higher transmission rates, weight savings, immunity to electromagnetic interference, and more energy efficient alternatives compared to copper wire cables or radio communication [1, 2]. Communication links often incorporate modulation for transmission of multiple signals over a band pass frequency simultaneously over a single channel, such as fiber or free space. Modulation is the process of imposing a signal, generally with information, onto another signal referred to as a carrier signal for transmission. Analog communication, although often not thought of as being advanced as digital communication, is prevalent in many applications including array antennas, satellite, radar, and RF communications [3]. The use of analog communication reduces bandwidth allocations for signals and is low cost when compared to digital communication [4].

1.1 Analog Photonic Links

Communication systems using analog photonic links to transfer information at rates of 100 GHz and higher have been demonstrated by others [5]. The simplified analog photonic link in Figure 1.1 depicts the major components used to transmit data.

Systems consist of a low frequency signal, typically DC-40 GHz, modulated onto an optical carrier at telecommunication wavelengths in the IR wavelengths of 1310 nm or 1550 nm and then transmitted with low propagation losses of 0.2 dB/km [6]. A channel such as optical fiber or free space is used to transmit the signal to a photodetector for demodulation.

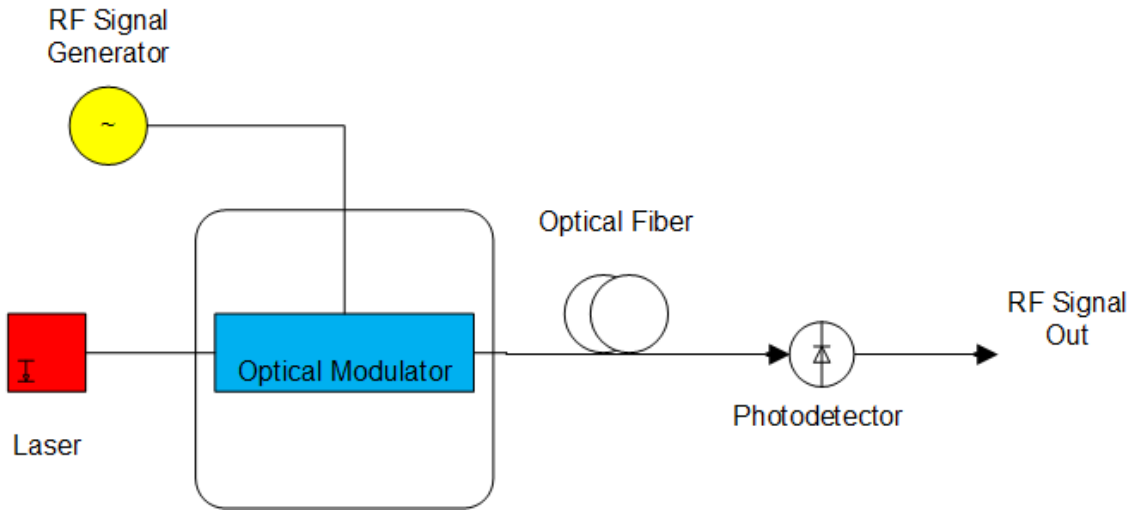

Figure 1.1: Analog Photonic Link

1.2 Optical Modulation

An area of research in analog photonic links is the modulation of electrical signals to the optical light seen by the optical modulator in Figure 1.1. This transfer of information is achieved by using analog modulation techniques such as amplitude, frequency, or phase modulation. Devices that modulate signals include Mach-Zehnder Interferometers (MZI), ring resonators, and optical switches [7]. In the case of phase modulation to make data transfer efficient, the half-wave voltage (V_π) of the modulating device must be low. The V_π of a device is the voltage required to change the phase of the light by π which allows for the signal to be modulated. To lower V_π, the sensitivity of refractive index (Δn) change can be increased when a voltage is applied. A refractive index change slows down light to cause constructive and destructive interference [8]. Increasing the electro-optic coefficient of interest in the electro-optic (EO) material known as the r_{33} increases the sensitivity of the index change with respect to applied voltage. With a long history of research in design lithium niobate ($LiNbO_3$) MZIs have been shown to have a V_π as low as 5 V at 40 GHz at telecommunication wavelengths [9].

1.3 Electro-Optic Polymers

The optical modulator is an important component in the analog photonic link and can be improved with the use of EO polymers due to their high electro-optic coefficient [10, 11, 12]. A V_π of 0.8 V has been demonstrated with EO polymers in their relatively short history of use in modulators [13]. The polymers themselves do not posses a high electro-optic coefficient so nonlinear chromophores are added to the polymer matrix in order to exhibit the desired electro-optic effect. To unlock the potential electro-optic coefficient of the polymer the film needs to undergo a process called poling. With the large r_{33} from chromophores there is a high propagation loss of 0.6-1.2 dB/cm [8] compared to $LiNbO_3$ at 0.17 dB/cm [14] which limits the physical size of devices [1]. For the majority of application the high loss is of no concern as the devices can be made less than a few centimeters in length.

Modulators made using EO polymers offer advantages such as low cost of fabrication, low driving voltage, fast electro-optic response time in the range of femto-seconds, low dielectric constant at desired microwave frequencies, and higher electro-optic coefficients [7]. Electro-optic polymers have as much as ten times the electro-optic effect of $LiNbO_3$ crystals that are widely used for optical modulation in industry [4]. Current $LiNbO_3$ technology performance degrades quickly after 40 GHz [6, 15]. The properties of these materials are reaching their limits for high frequency operation

[10, 16] while electro-optic polymers have been demonstrated to operate at 110 GHz [17] and even as high as 200 GHz [5, 17]. Increasing the frequency bandwidth allows for communication in frequencies with less traffic that reduce interference and distortion along with higher bandwidth availability. In the high frequency domain there are reductions in the dimensions for components and antennas in wireless communication applications [7]. EO polymer devices have the benefit of operating in the high frequencies provided by references. EO polymer devices operating as antennas can also be fabricated with smaller dimensions that correspond to high frequencies as defined in Equation 1.1 with a low V_π due to their high electro-optic coefficient. The operating frequency of the antenna is inversely proportional to the wavelength. In Equation 1.1 λ is the wavelength expressed in length, c is the speed of light, and f is the frequency.

$$\lambda = \frac{c}{f} \tag{1.1}$$

One promising EO polymer SEO100C offered by Soluxra, LLC has been demonstrated to have an r_{33} of 140 pm/V after thin film poling [18, 19]. An r_{33} of 226 pm/V in multi-layer thin film devices has also been reported [20]. Coefficients in excess of 500 pm/V have been reported in polymer materials, but have not been reported in thin film waveguide devices [21, 22]. Through laboratory design and configuration SEO100C thin films were poled and validated at Michigan Technological University

using index of refraction shifts. Future device testing has been designed, configured, and validated using a commercial Mach-Zehnder modulator.

1.4 Fabrication of Devices

Integrated EO polymer modulators are fabricated by creating thin film waveguide devices. Figure 1.2 shows typical processing steps of fabricating a raised rib thin film EO device. An inverted rib structure can also be realized by etching waveguides into the bottom cladding material and filling the trenches with EO polymer. The feasibility of fabrication for each structure is determined by chemical interactions, feature resolution, and layer etching. By no means is the fabrication process trivial to replicate due to many tolerances in design, material, and processing. Small deviations or changes in the recipe impact the final device and the resultant r_{33}.

Important factors in the fabrication process are adhesion properties, reproducibility, and propagation and coupling losses [23]. Steps 3, 4, and 9 of Figure 1.2 are important for consistent uniform thickness over the device which effects maximum voltage levels and poling uniformity. There are points in the process that are susceptible to imperfections forming in between layers that limit the maximum voltage that can be applied. Even the specific processing details in filtering, spinning, curing, and temperature processing can change the material properties including adhesion and

resistivity values [24].

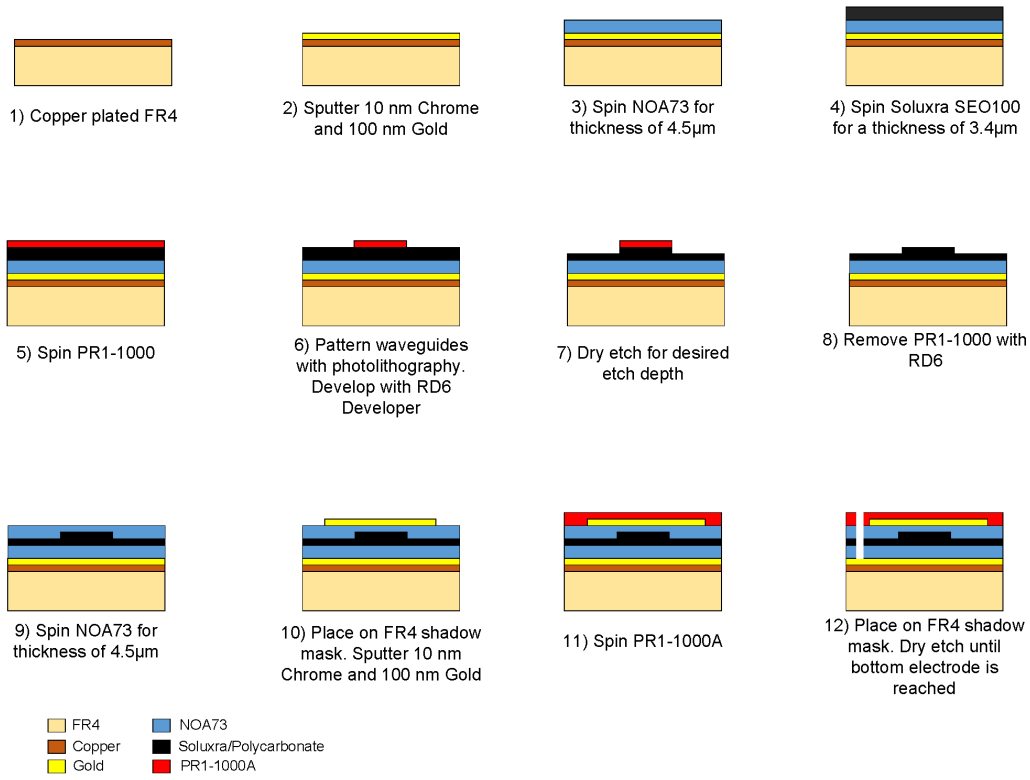

Figure 1.2: Fabrication flowchart of device on FR4

A dicing saw is used to expose the waveguide end faces. Careful consideration of dicing parameters are needed to reduce delamination of the thin film from the substrate and insertion losses caused by roughness of the cut surface. After dicing, the electro-optic poling of the device is used to develop a high r_{33} of the polymer waveguide material. The poling process is crucial as it exposes the device to high temperatures and electric fields making the device susceptible to dielectric breakdown.

Chapter 2

Electro-Optic Coefficient

The electro-optic coefficient of a material affects phase shift sensitivity of light as it passes through regions activated by an applied electric field. A large electro-optic coefficient can reduce component size and drive voltage of modulating devices [10]. Increase in the electro-optic coefficient of polymer materials is correlated to high propagation loss, but can be countered by shorter dimensions of waveguides in devices due to the same coefficient [23, 25].

Measurement techniques for the electro-optic coefficient for simple thin films and multi-layer devices are discussed for each. Measurement is used to validate that the thin film polymer has had an increased electro-optic coefficient after all fabrication steps have been been completed.

2.1 Electro-Optic Theory

The pockels (r_{33}) and kerr (r_{13}) effects define the ability of the index of refraction to be varied from an applied voltage. The linear r_{33} coefficient is of primary concern [26] for fabricated devices. The quadratic r_{13} coefficient also exists, but is neglected due to its scalar magnitude in relation to r_{33} [23].

The pockels effect seen in equation (2.1) shows the positive relationship of the r_{33} and change in index Δn [21]. The electric field is desired to be as low as possible for a change in index relating to a phase shift of π. A higher sensitivity to the electric field can be shown by increasing r_{33} gives fabricated devices higher performance.

$$\Delta n = \frac{n^3 r_{33} E}{2d} \tag{2.1}$$

2.2 Electro-Optic Thin Films

Thin film EO polymers are spun on indium tin oxide (ITO) glass slides with chrome and gold deposited top electrodes. Once poled the top electrode has been removed through a wet etch, the film is exposed for measurement. Because of the accessibility of the film these measurement techniques bypass the need for coupling into waveguides

at the end faces. In this respect, measuring thin film EO polymers is more straight forward than measurement of multi-layer devices.

2.2.1 Prism Coupler (Δn)

The electro-optic coefficient of a poled film can be measured using different methods with the correct setup and instruments. These methods include attenuated total internal reflection, MZIs, Michelson interferometers, Fabry Perot resonators, and finally, the Teng-Man method which is the most widely used [27, 28, 29].

The index of refraction change in SEO100C is used to confirm poling of thin films to validate the experimental poling setup. Poled SEO100C shows a difference in index of refraction compared to non-poled thin film samples. To measure the index of refraction a Metriocon model 2010 prism coupler, shown in Figure 2.1, with a wavelength of 1543 nm is used to closely match that of the 1550 nm telecommunication wavelength.

Figure 2.1: Metricon model 2010 prism coupler

Light is coupled into the thin film using a prism to achieve total internal reflection (TIR) [30, 31, 32]. When this occurs a power detector level reaches a minimum and is correlated with an angle of incident. This angle is used to calculate the index of TE and TM modes polarizations. Measurement using the prism coupler is not possible with the multi-stack structure because of the layers with different index of refraction [31, 33].

$$\beta = \frac{2\pi n_{prism} \sin(\theta)}{\lambda} \tag{2.2}$$

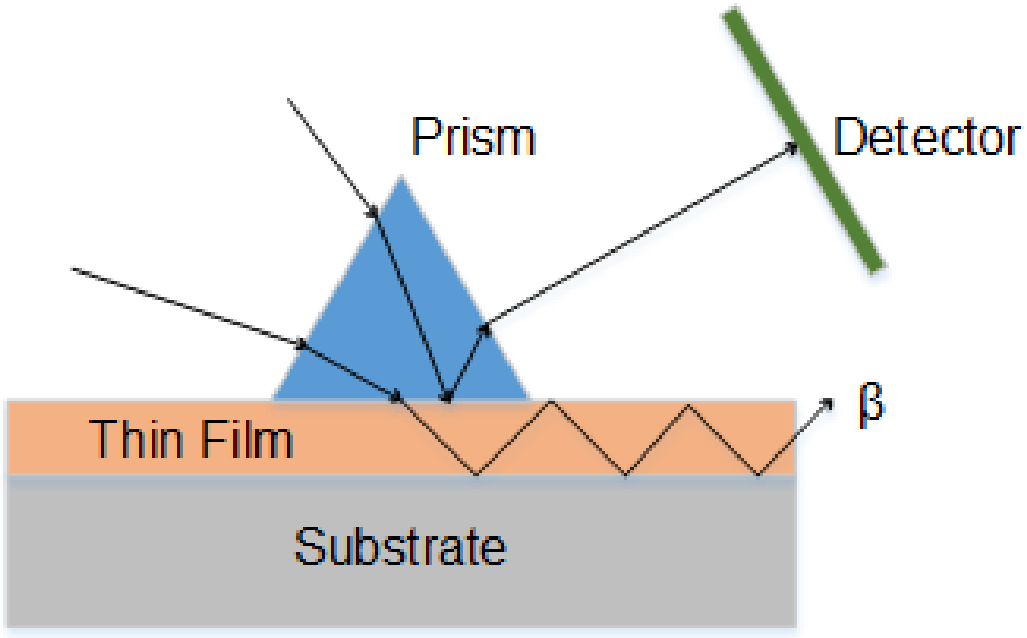

Figure 2.2: Prism coupler operation

Light is coupled onto the thin film by placing a prism with an index of refraction (n_{prism}) greater than that of the thin film under test. Values were chosen to be 2.6942 and 2.4440 for TE and TM indexes respectively compared to 1.65 and 1.70 of Soluxra at a wavelength of 1330 nm [18, 32]. The prism is placed in contact with the sample used to couple a laser with 1543 nm wavelength (λ) into the thin film. The sample and prism shown in Figure 2.3 rotate on a stage to find an angle θ at which light is coupled into the thin film. When the detector power level reaches a local minimum the laser is coupled into the thin film as the light mode propagates

(β) through the film and away from the detector. The phase matching condition is satisfied due to $n_{substrate} < \frac{\beta\lambda}{2\pi} < n_{film}$ from Equation 2.2 and indicates locations of mode propagating within the film. If only one mode is found, the thickness of the film is needed to calculate the index of refraction [23]. When two or more modes are found in the thin film the film thickness and the index of refraction of the fundamental mode can be calculated. Figure 2.2 shows two incoming rays of light at different angles and how they interact with the prism and thin film. The TM polarization is of primary concern as the fabricated devices are designed to work in the TM polarization.

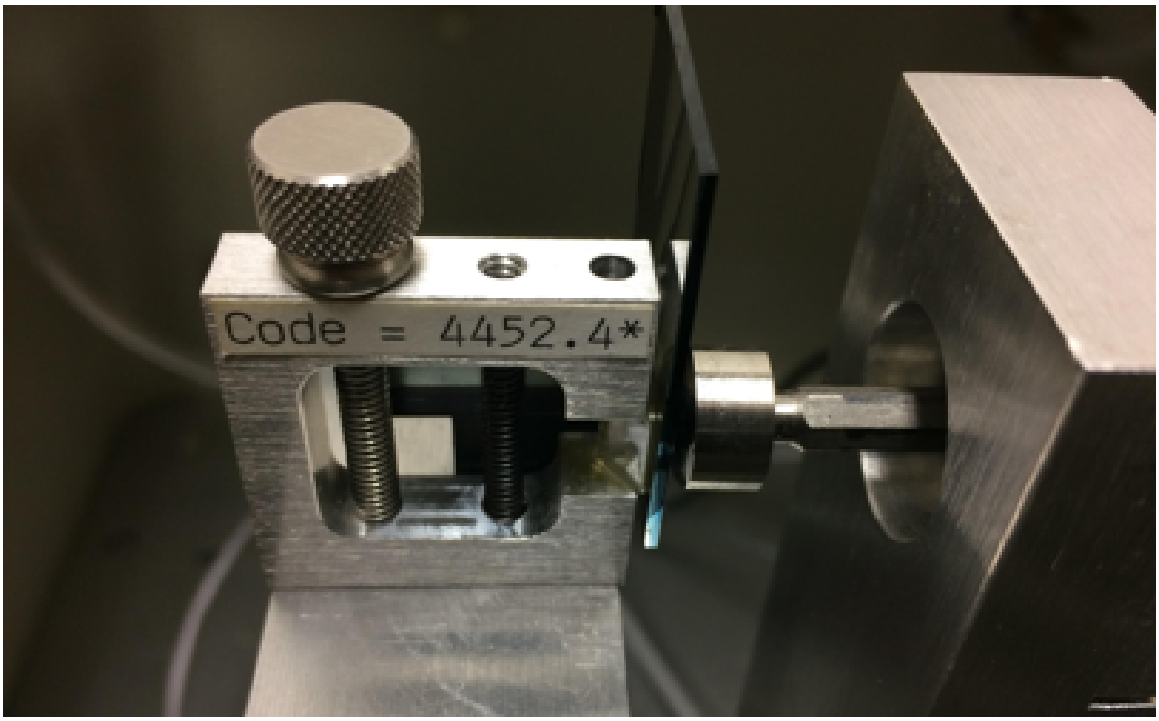

Figure 2.3: Sample mounted in prism coupler

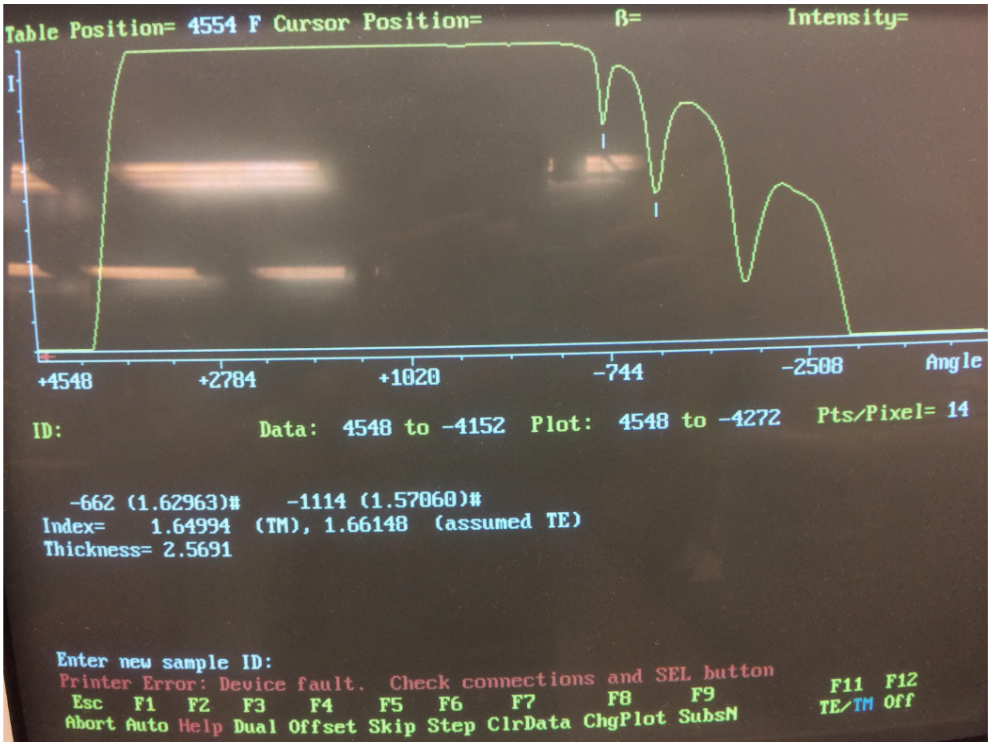

Figure 2.4: Sample SEO100C data obtained from prism coupler

As an example, a screen capture of the SEO100C thin film index of refraction measurement is seen in Figure 2.4. The local minimum in power measured by intensity on the y-axis correspond to angles on the x-axis used for index and thickness measurements.

2.2.2 Teng-Man Method (r_{33})

The Teng-Man method can be used to measure both the pockel's and kerr effect from a thin film sample [27, 34]. Equations 2.3 and 2.4 can be used with gathered data

from the Teng-Man method to determine the electro-optic coefficients [27].

$$\Delta n_o = -\frac{n_o^3 r_{13} E}{2} \tag{2.3}$$

$$\Delta n_e = -\frac{n_e^3 r_{33} E}{2} \tag{2.4}$$

The Teng-Man method setup up is shown in Figure 2.5. Individual components of the setup are expensive and physical connections to the top electrode and ground to the signal generator will be required on the sample. The Teng-Man method is the most commonly used measurement for electro-optic coefficients of thin films [27, 35]. Prism coupling measurements of the index of refraction can be used to correlate the increase in the electro-optic coefficient and poling due to the costs and potential setup complications [36].

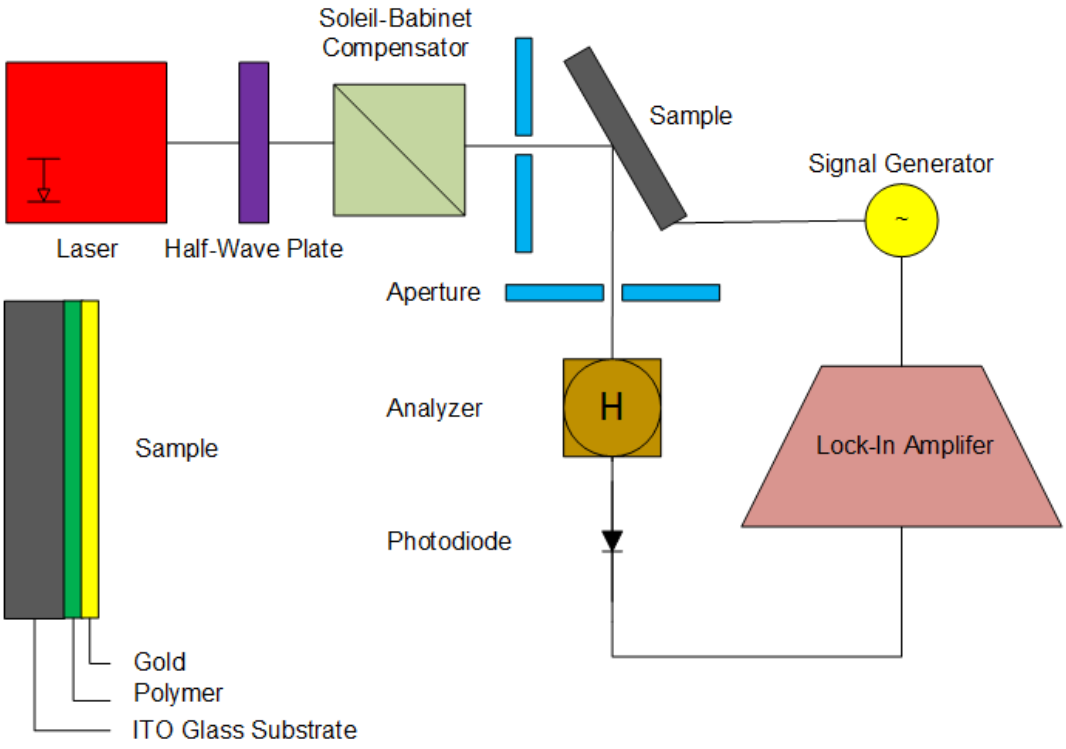

Figure 2.5: Teng-Man method setup

2.3 Multi-Layer Device

When poling devices with multiple layers the core layer cannot be measured using the prism coupler due to the top cladding layer limiting access to the core layer [10]. Instead, if a device is fabricated, such as a Mach-Zehnder modulator, the V_π can be measured and used to calculate the r_{33} electro-optic coefficient by coupling light.

2.3.1 Half-Wave Voltage (V_π)

The V_π is the voltage required to induce a phase change of π in light propagating through the material. V_π is determined by dimensional and material characteristics seen in Equation (2.5) [10]. Minimization of the V_π value is desired so the device can go from zero to full transmission with minimal power [10, 25].

$$V_\pi = \frac{\lambda d}{2n^3 r_{33} L \Gamma} \tag{2.5}$$

For fabricated devices the wavelength (λ) is that of the incoming light source, film thickness (d) is the EO polymer core thickness, refractive index (n) is a material property, length (L) is the length of electro-optically active polymer, and the overlap integral (Γ) assumed to be 0.5 accounts for overlap of the modulating electric field with the optical mode. The V_π is measured by incremental voltage levels on the device until a phase change of π is seen. The r_{33} coefficient can then be calculated from designed dimensions of the device.

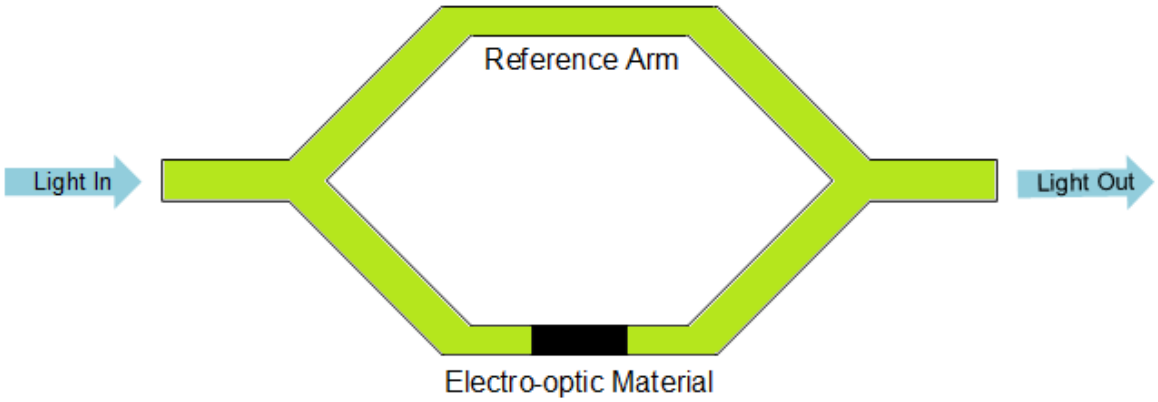

Figure 2.6: Diagram of a Mach-Zehnder interferometer

The MZI is a common device that uses V_π as a unit of metric. The MZI splits guided light using a Y-junction into tow arms shown in Figure 2.6. Using electrodes and the electro-optic effect, the phase in the control arm is shifted while the reference arm is unaffected. Once recombined using another Y-junction the amplitude can be measured for constructive or deconstructive interference. The voltage required to move from minimal power to maximum power is measured as the V_π of the device [23].

Chapter 3

Electro-Optic Poling

Electro-optic poling is a crucial step after fabrication of EO polymer thin film devices. The nonlinear chromophores that are suspended in the polymer host have an insignificant electro-optic coefficient when not aligned [21, 37]. Before poling the electro-optic effect discussed in Chapter 2 is weak and the performance of the device would not be a viable modulation device.

3.1 Electro-Optic Poling Theory

Electro-optic poling is the process of increasing the electro-optic coefficient of a material through thermal and electric field stimulation. With a stronger electric field, the

alignment efficiency of chromophores increases and therefore increases the r_{33} of the material [34]. The capability of EO polymers to have electro-optic coefficient significantly higher than $LiNbO_3$ crystals, into the range of a few hundred pm/V, can offer more compact and energy efficient devices. To reach high values of r_{33}, the polymer must be poled to align chromophore dipole molecules within its structure. These chromophores are randomly orientated during mixing and spin coating of the thin film. The chromophores are aligned using an applied electric field shown in Figure 3.1, but first the molecules must be freed from their immobile state. In order to have efficient poling the polymer is heated to its glass transition temperature (T_g) where chromophores are allowed to rotate more freely and align parallel with the influnce of an applied electric field. The polymer is then cooled to room temperature and the electric field is removed so that the chromophores remained fixed in their new positions [38].

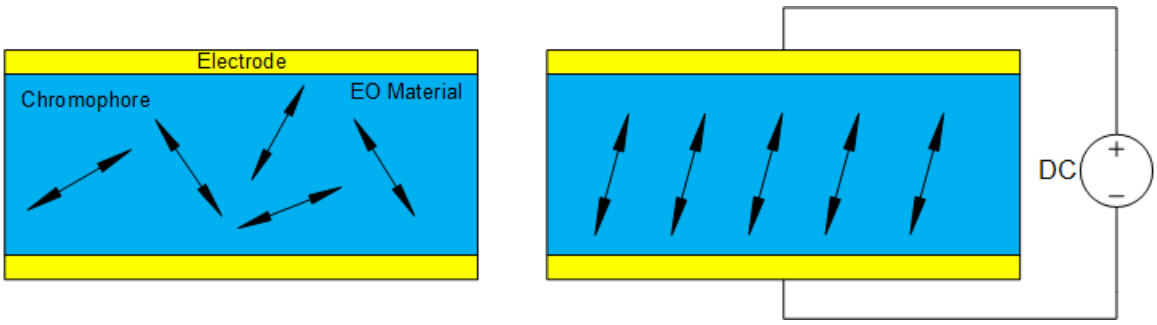

Figure 3.1: Alignment of chromophores due to an applied Electric Field

In order for an analog optical modulator to operate, the index of refraction of the waveguide material must vary when an electric field is applied. There is a larger

change of the index per volt with a larger electro-optic pockel's coefficient (r_{33}) reported in pico-meters per volt (pm/V). The r_{33} value in polymers can increase significantly with values up to ten fold of $LiNbO_3$ crystals when poled [6].

3.2 Thin Films

Thin films are used for validation of the electro-optic poling setup and prism coupler measurements. These thin films are much more sensitive to physical damage than the multi-layer devices without protection from the cladding layers. Pressure from placing the voltage probes and contact while measuring the film using the prism coupler are the major concerns.

3.2.1 Sample Preparation

Thin film polymers are spun onto ITO glass slides using spin curves of the polymer as a guide for their thickness. Before poling initial measurements are made using the prism coupler. A top electrode of chrome and gold are deposited and defines the poling region as the conductive ITO covers the entire bottom of the glass slide. If there are defects such as pinholes, for example, in the poling region of the thin film, damage will occur at minimal voltages and poling will not occur. Once poling is

complete, the top electrodes are removed using wet etching techniques and the film is remeasured.

3.3 Multi-Layer Devices

Multi-layer devices are more robust than the thin films, but there is careful consideration of the handling of end faces of waveguides after dicing. After fabrication, devices are ready for electro-optic poling with the top electrode again defining the poling region. The extra cladding layers allow for higher voltages to be used with mitigation to pin-hole defects. Measurement of the film cannot be done from the top of the film due to these layers and light must be coupled for device characteristics.

3.3.1 Sample Preparation

The sample can be mounted directly into the the poling setup. Imperfections within layers can be viewed from the top of the device, but cannot be used as a true indication of where dielectric breakdown may occur or at what voltage. Pressure from placing the voltage probes on the top electrode may cause damage to the electrode. This damage can be mitigated by using micro-manipulators to lightly touch the top electrode surface with a probe tip.

3.3.2 Resistivity of Layers

When adapting thin film electro-optic poling to completed multi-layered device structures, the voltage field over each material must to be taken into account. In thin film electro-optic poling the input voltage is completely applied to the EO material in between the top and bottom electrodes. When introducing stacked layers in a device the voltage across the EO material follows from the voltage divider rule seen in Equation (3.1) with three resistors in series. Electrode layers have negligible resistances and therefore are omitted from the calculation.

$$V_2 = \frac{Z_2}{Z_1 + Z_2 + Z_3} V_{in} \tag{3.1}$$

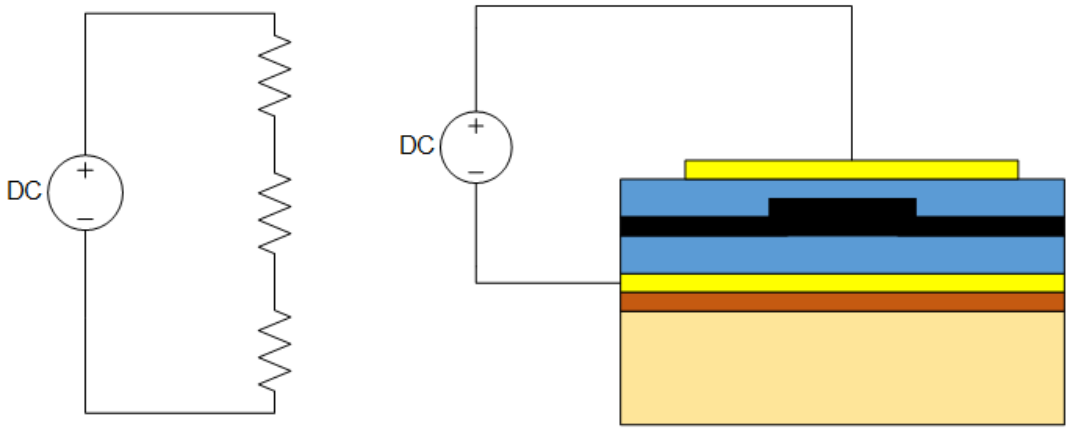

Figure 3.2: Voltage divided among layers in the device

In a three layer stack each material can be represented with a resistance value depicted in Figure 3.2. The resistance of thin films is determined by area, thickness, and material properties. The material properties can change based on exact fabrication procedures. The area and thickness can vary slightly based on device specifications and processing. Since it is impractical to measure resistance for each layer, the resistivity of each material is used to determine the ratio of voltage applied to the device and the voltage field over the EO material. Since the same cladding material is used on either side of the core material, Equation (3.2) can be used. Voltage is denoted by V, ρ is resistivity, and d is the layer thickness while, core and clad represent the EO polymer and the cladding layers respectively.

$$V_{total} = V_{core}[\frac{\rho_{core} + 2\rho_{clad}(\frac{d_{clad}}{d_{core}})}{\rho_{core}}] \tag{3.2}$$

If the resistivity of the core is orders of magnitude higher than the cladding material, the voltage field over the core will approach the applied voltage to the device [39, 40, 41]. The resistivity of NOA73 and UV15LV were experimentally measured based off of processing parameters. Due to the limited supply of Soluxra SEO100C, data sheets from the manufacturer were used to provide values to calculate its resistivity.

Preliminary surface resistivity measurements were attempted using a four point probe station for film resistivity. The four point probe uses four evenly spaced wires that

are placed in contact with the sample material. Current is applied to the outer two probes and voltage is measured between the inner two probes. The resistivity can be shown by the Equation (3.3) below where d is thickness and is independent of probe spacing.

$$\rho = \frac{\pi d}{\ln(2)}(\frac{V}{I}) \tag{3.3}$$

Because of the high resistivity values of the materials and the lab's measurement capabilities, values of voltage from the four point probe station were not not in measurable range. The next option was the use of a Keithley 4200A-SCS Parameter Analyzer to acquire IV curves of from small gold pads on square samples. This again produced unreliable results due to the low signal level being acquired. For more reliable results 4-inch RCA cleaned wafers with chrome and gold at 10 nm and 100 nm respectively were spun with NOA73 and UV15LV then UV (ultra-violet) cured. The UV15LV was filtered using a 0.4 μm pore size to remove impurities in the sample. Bottom electrode access points were taped off using Kapton tape. FR4 masks were used with varying radii for the top electrodes to be sputtered with chrome and gold at 10 nm and 100 nm respectively seen in Figure 3.3. A larger pad size was used for the NOA73 since the resistivity is cited to be in the order of magnitude of 10^{10} Ωcm. UV15LV is cited to have a resistivity in the order of magnitude of 10^{9} Ωcm.

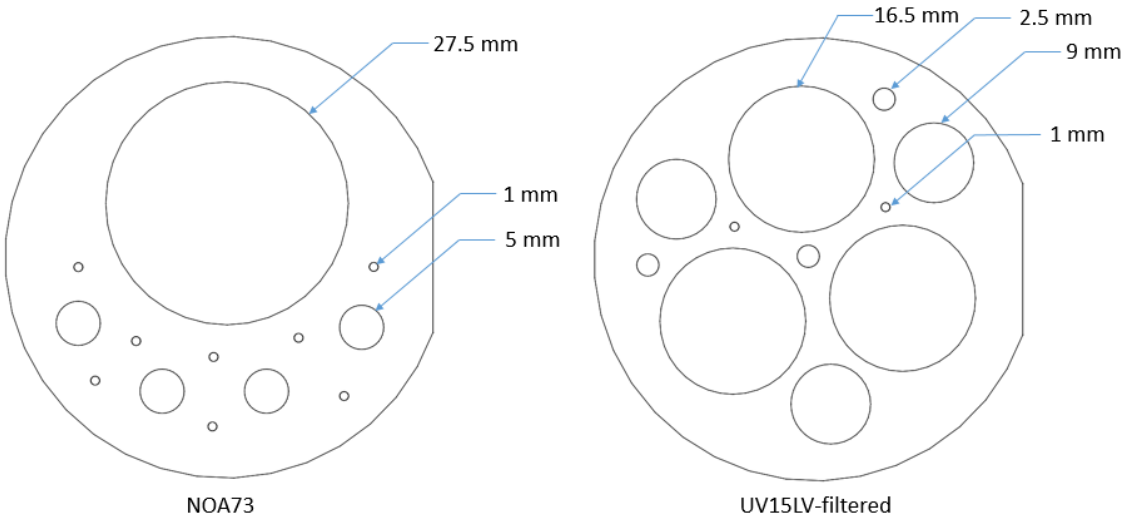

Figure 3.3: FR4 mask designs with gold pad radii for resistivity measurements

Samples were placed on a hotplate and heated to 135°C during the measurement to mimic temperatures during poling. The surface temperature is 135°C when set to 160°C as seen in Figure 3.4. The resistivity was found from the I-V curves using Equation (3.4). Sample curves are provided in the Appendix A.1 and A.2. Resistivity values were tabularized with measured results and results found from various journals and data sheets in Table 3.1.

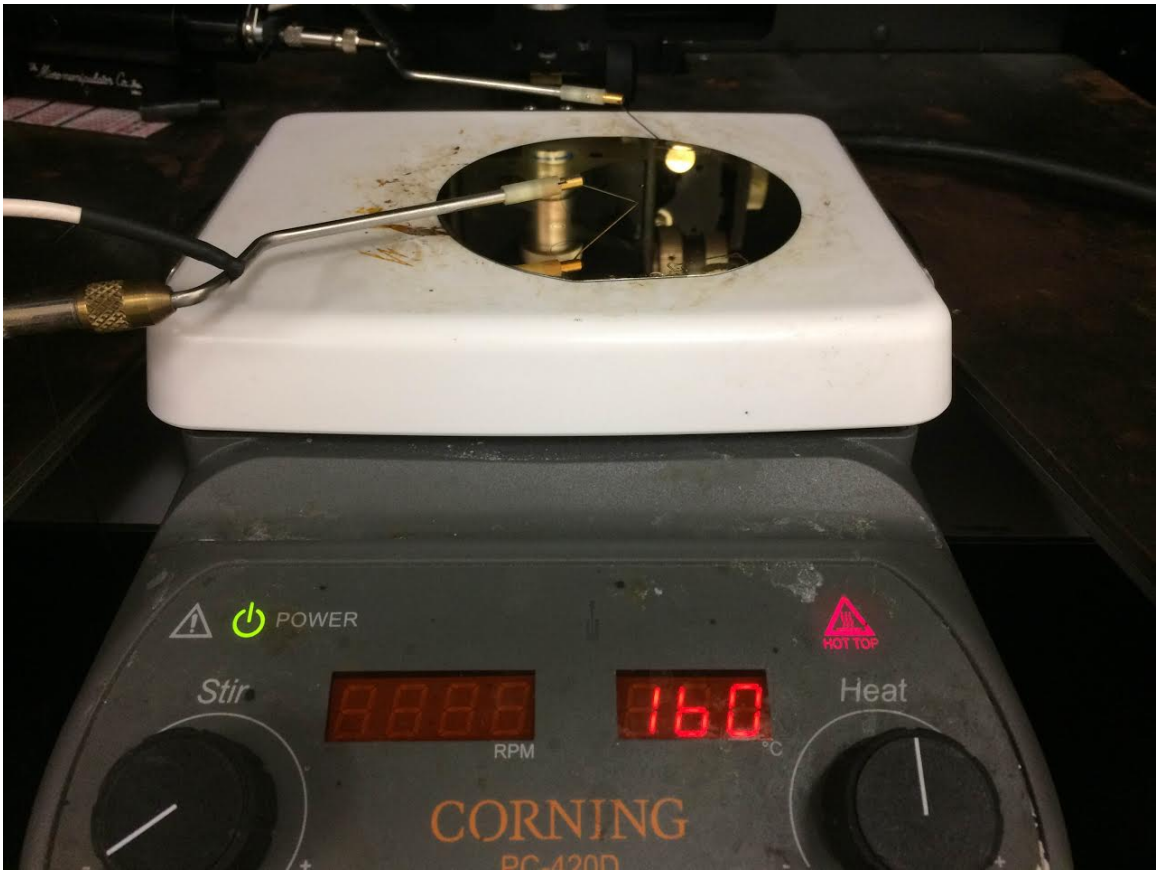

Figure 3.4: Resistivity sample on hot plate at a surface temperature of 135°C during testing

$$\frac{V}{I} = R = \frac{\rho d}{A} \tag{3.4}$$

Table 3.1
Resistivity findings from IV curves, journal articles, and data sheets in [Ωcm]

Measured (135°C)	**Journal Articles**	**Soluxra, LLC (135°C)**
NOA73: $3.3 * 10^{10}$	NOA73: $2.5 * 10^{9}$ (130°C)[42]	SEO100C: $3.0 * 10^{10}$[18]
UV15LV-filt: $3.4 * 10^{8}$	NOA73: $1.2 * 10^{10}$ (200°C)[43]	SEO125B: $1.2 * 10^{10}$[44]
	UV15 and NOA73: 10^{10} (130°C) [24]	
	UV15: 10^{12} (90°C) [45]	
	SEO100C: $5 * 10^{11}$ (130°C) [46]	

Using Equation 3.2 for poling voltage across SEO100C of 100 V/μm and a thickness of 3.4 μm along with NOA73 having a thickness of 4.5 μm, the total voltage comes to 1330 V. Accurate resistivity values of SEO100C in similar processing conditions need to be measured to increase the accuracy of Equation (3.2).

There are many challenges when measuring high resistivity thin film materials. These highly resistive materials pose a challenge when trying to take resistivity measurements. Standard 4-probe tests cannot be used as the voltage levels are below the measurement capabilities of most equipment. Two probe tests should have the material spun on top of a conducting guarded electrode and an additional top electrode with a large area to allow for enough current to pass through while reducing surface

conduction effects [42]. In addition it is desirable to measure the resistivity of the material in a similar environment as poling (i.e. 135°C and 100 V/μm).

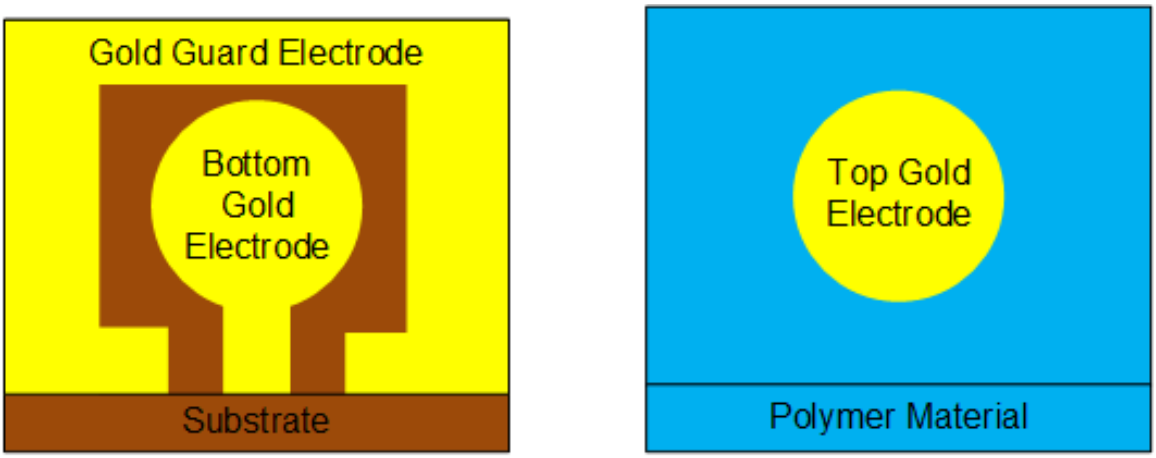

Figure 3.5: Proper sample preparation to prevent fringing effects

During the fabrication of the test sample there is always a chance for particulates or imperfections to enter into the layers. Imperfections increase the possibility of electrical shorting and is more likely due to the large electrode area. This large area also allows for thickness uniformity to become a concern as electrical current will pool in thinner regions. Fringing effects from the fully coated bottom electrode were neglected in the resistivity measurement. A proper setup to reduce these fringing effects would be to lay down a guarded bottom electrode as seen Figure 3.5 from work done by Emily M. Heckman and Perry P. Yaney [41, 42].

3.4 Electro-Optic Poling Procedure

The procedure for electro-optic poling is simple in concept and can be visualized in Figure 3.6. The sample is initially heated to a temperature for constant processing before an applied electric field is applied. The strength of the electric field is chosen to produce a strong desired r_{33} coefficient in the EO polymer while maintaining a high yield. The sample is heated to T_g of the polymer to allow for chromophore alignment to the electric field. The sample is then cooled before the electric field is removed.

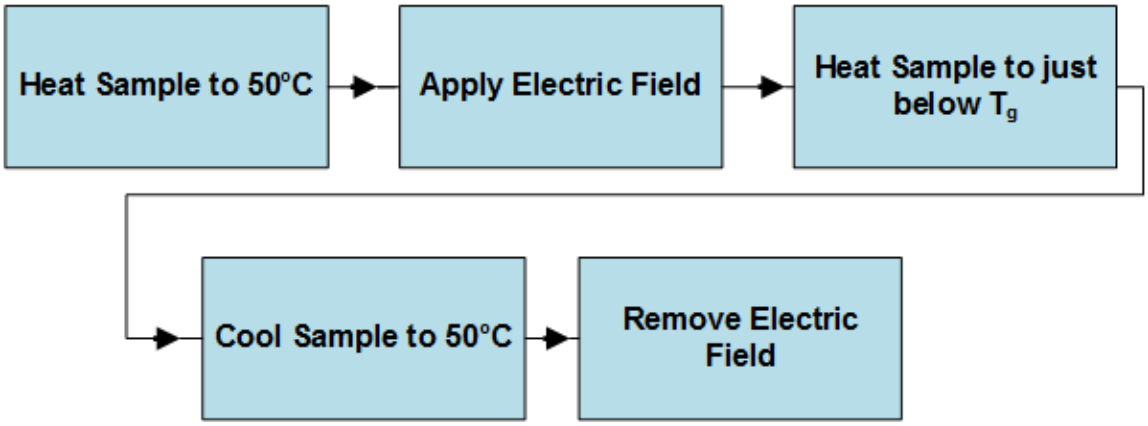

Figure 3.6: Poling flowchart

The process shown in Figure 3.6 is the same for thin films and multi-layer devices. Finer details in sample mounting, heating, and connection of the electric field are supplied in Section 3.5.

3.5 Electro-Optic Poling Setup

Electro-optic poling requires the use of an oven to increase temperature of the sample at a constant rate and a high voltage source. A pico-ammeter is inserted into the setup to record current increases during the process. Temperature and current data are recorded using a LabVIEW VI file into Excel.

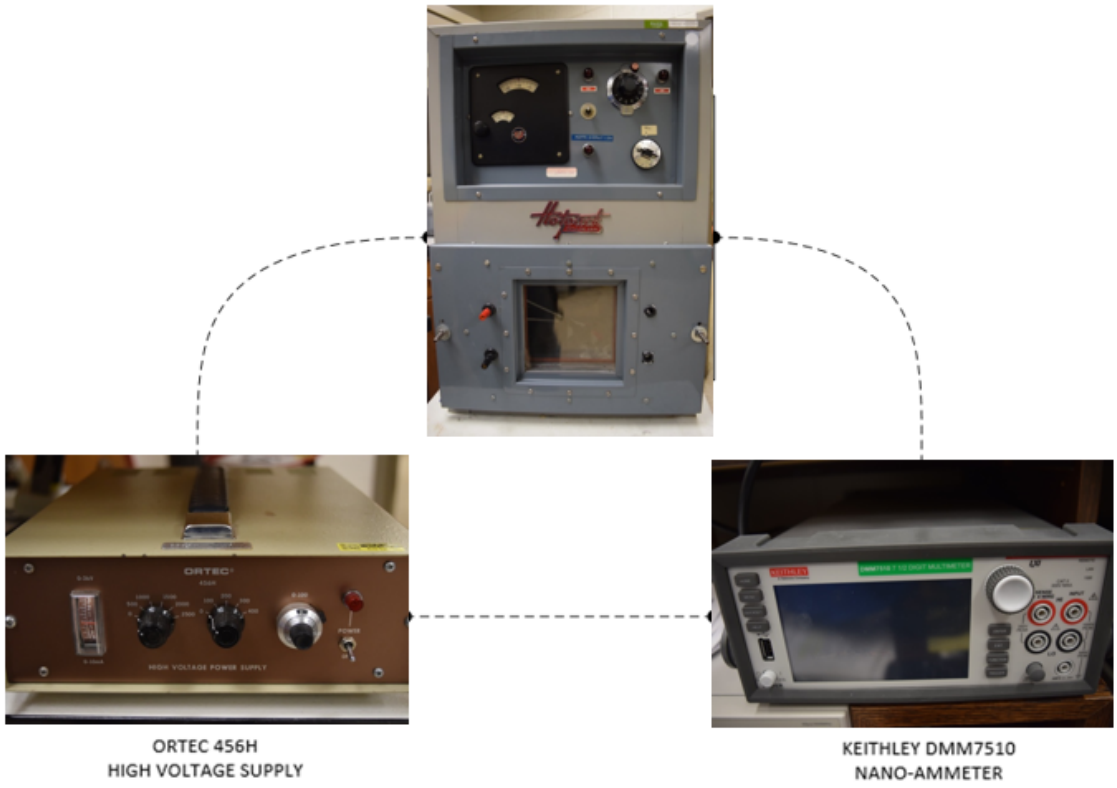

Figure 3.7: Physical poling setup

The configuration of poling can be seen in Figure 3.7. The oven allows for ±5°C stability, a variable temperature rate while heating, and modification to allow for

high voltage electrical connection. The Ortec 456H high voltage supply allows for up to a 3000 V electric field. The Keithley DMM7510 allows for current to be measured with a resolution of a pico-amperage. Temperature is measured using a K-type thermocouple wire with a washer mount seated near the sample in a clamp with a measurement accuracy of $\pm 0.5°C$. Accurate monitoring of the temperature is important when the oven is near T_g of the SEO100C material to prevent damage from dielectric breakdown. A National Instruments DAQ USB-6009 measures the voltage from the thermocouple and is input into the LabVIEW VI along with the current from the DMM7510. Drivers and VIs were updated to incorporate a Keithley 4685 pico-ammeter to replace the DMM7510 and has similar specifications.

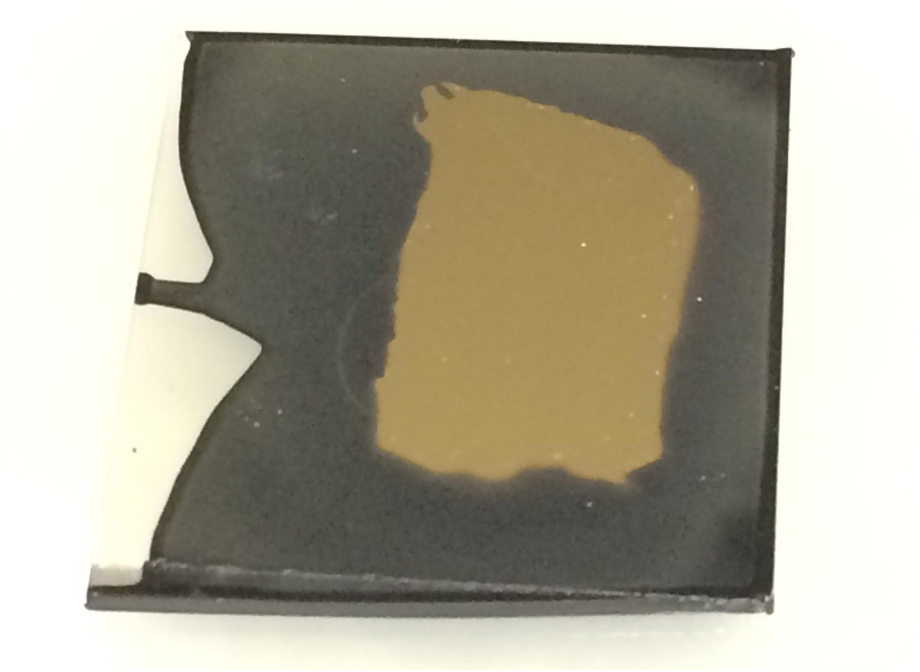

Figure 3.8: SEO100C thin film

Thin film samples of SEO100C were poled on ITO glass slides with a top chrome and gold electrode of 10 nm and 100 nm respectively, shown in Figure 3.8. Devices with stacked layers have access to the top and bottom electrodes for contact. It is important to note that there must be spacing between the top electrode and the edge of the diced sample if the bottom electrode covers the entire substrate. This spacing is set to be greater than one millimeter to prevent flash over or arching at the diced edge while applying high voltage. The contact of the applied voltage and the electrodes was done in two ways.

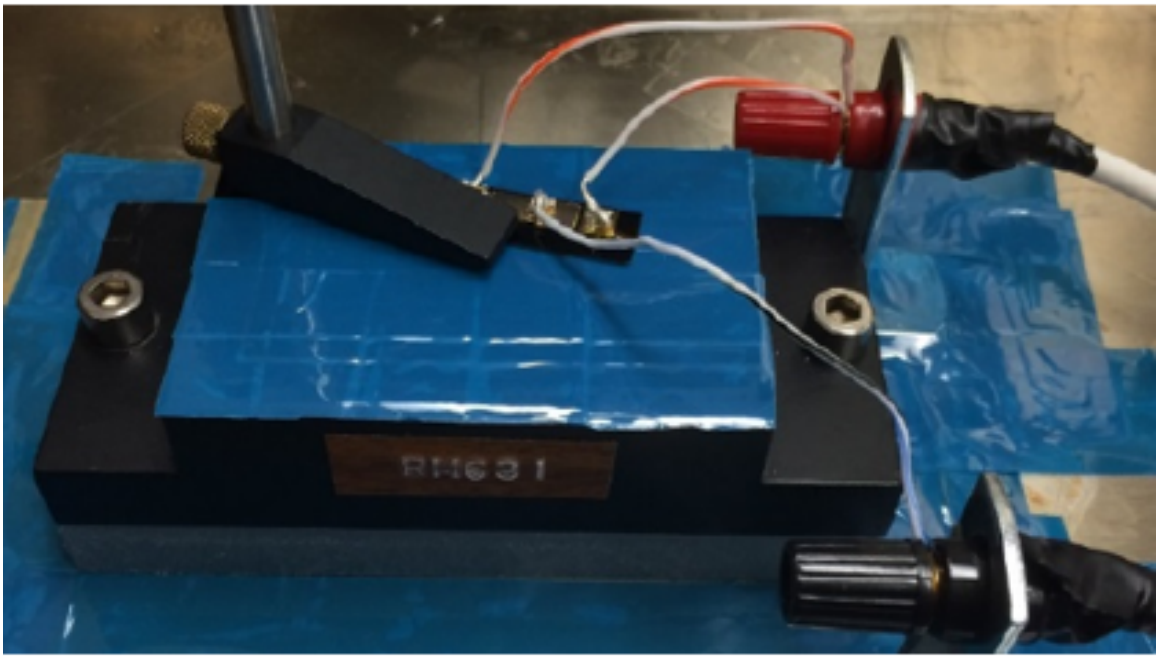

Figure 3.9: Initial connection to Mach-Zehnder sample using silver epoxy

The first method used silver epoxy to attach high voltage wires to posts leading outside the oven seen in Figure 3.9. The silver epoxy brought issues to the poling

process such as curing time, sparking at high voltages, and contact to small pad areas. The cure time takes 12 hours to complete before the contact is rigid enough to be handled. Once the heat and high voltage are applied the silver epoxy had a tendency to spark and be damaged enough to loose adhesion with the electrodes. Keeping in mind the spacing required to prevent arching from top to bottom electrode the epoxy should stay within the bounds of the pad. This spacing can be difficult as the pad size decreases for more efficient spacing of devices.

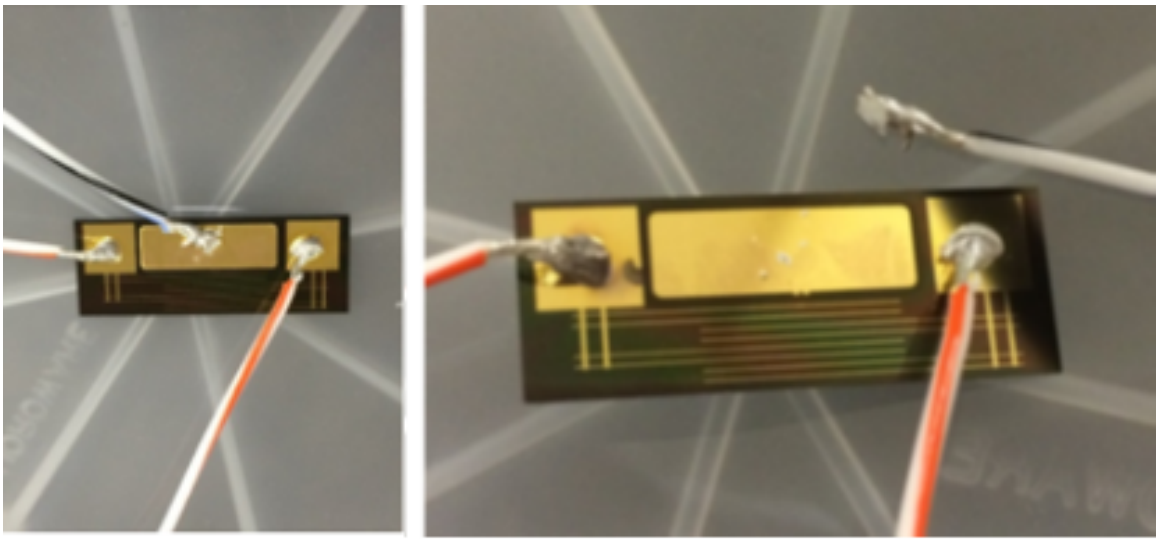

Figure 3.10: Attached leads before poling (left). Detached lead during poling (right)

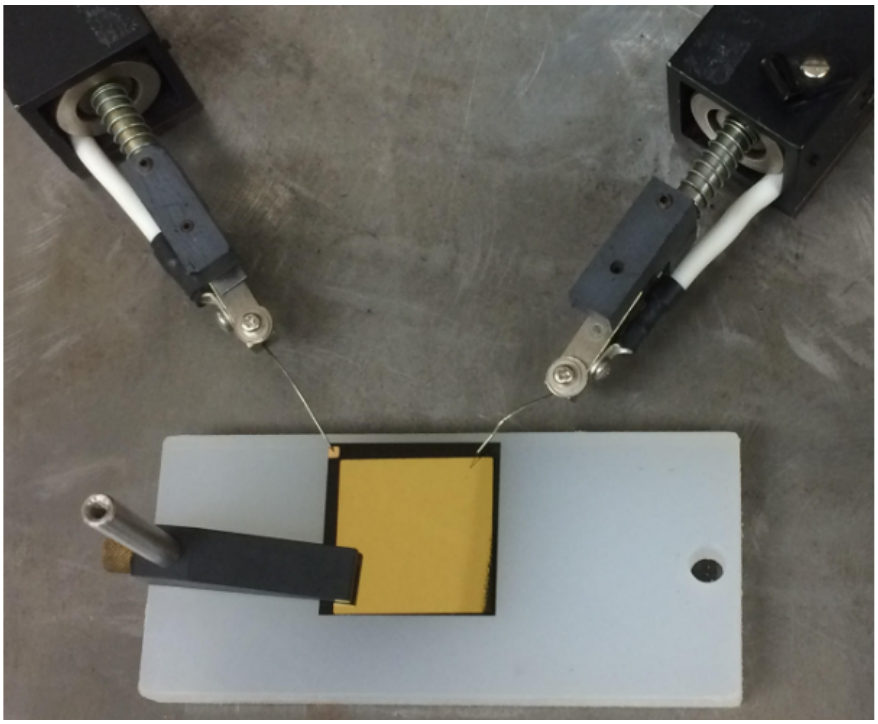

Figure 3.11: Current connection to radial bend sample with probes

Use of silver epoxy for attaching the leads to the devices allows for poling and measurement, but on occasion the epoxy peeled off during poling. This is due to mechanical strain and thermal increases of the connection. In Figure 3.10 the bottom electrode peeled off during poling resulting in a failed poling attempt. The wire can be reattached and cured, but the damage is usually extensive enough to ruin the sample for future testing. It can also be seen in Figure 3.10 that the positive electrode experienced an electrical shorting of the leads and cased an arch of spark to damage the device. In extreme cases the top gold electrode peeled off with some of the SEO100C material; permanently damaging the sample by an electrical short.

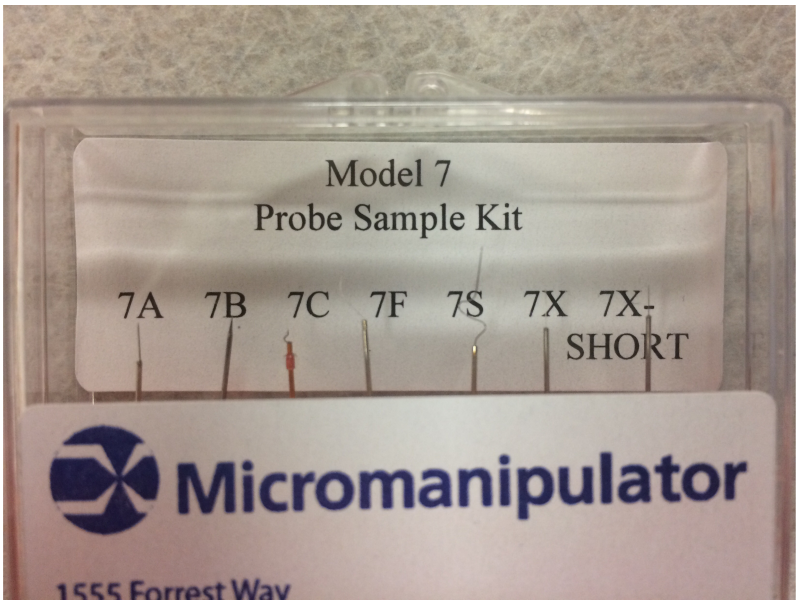

Figure 3.12: Probe Tips from Micro-manipulator

The second method used micro-manipulator probes to come in contact with the top and bottom electrodes allowing for secure contact and higher voltages as seen in Figure 3.11. The probes and mounting stage are secured to the oven using magnetic bases to ensure constant reliable contact between the probes and electrodes. Probe tips were carefully selected to withstand the high voltages and have the desired rigidity. Using thin flexible tips, such as the 7F from Micromanipulators Model 7 probe sample kit in Figure 3.12, cannot withstand voltages over 100 V. A 7B probe tip is used for the bottom electrode with a ridged body because there is no worry about puncturing past the electrode and into the layers below. The 7A probe is used for the top electrode that can withstand high voltage past 1600 V but with more flexibility to prevent puncturing. The probe method allows for higher voltage, smaller pad size, immediate

poling, and allows electro-optic poling without silver epoxy residue on gold electrodes when desired.

3.6 Electro-Optic Poling Current and Temperature Curves

Initial evidence that poling occurred in the sample can be obtained by observing a current and temperature curve over the poling process [39]. Once poling is complete the index of refraction step change in thin films, or the half-wave voltage in multi-layer devices, can be used. The parameter that is most valuable to obtain for device characterization is the r_{33} coefficient. Balancing the increase in the electro-optic coefficient with the yield is important to consider when using high voltage that is capable of damaging the sample.

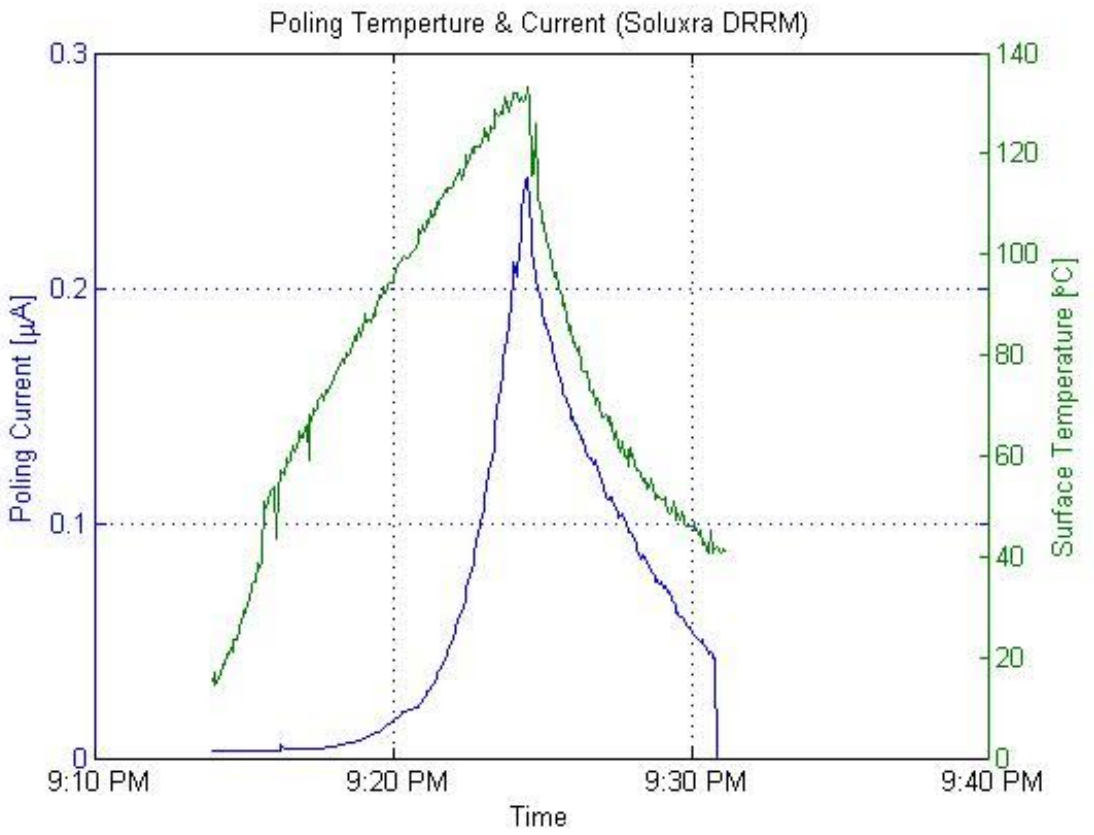

Figure 3.13: Data collected from poling of a DRRM device at 1200 V

Data collected from the LabVIEW VI during poling is exported to Excel and imported into MATLAB for plotting. Figure 3.13 shows temperature and current data collected from a alternative ring resonator device (DRRM) poled at 1200 V. Examples of collected data from Mach-Zehnder devices and a thin film are shown in Appendix B.1, B.2, and B.3. Spikes in current during the cool down period occurred when opening the door of the oven to let the sample cool down quicker. The higher current is an indication of more effective poling as long as there is no dielectric breakdown of the material to damage the sample. The voltage is left constant as the temperature

is increased from 50°C to 135°C and back down to 50°C.

The voltage applied to the device is directly proportional to the voltage field that the polymer experiences using the voltage divider rule. Applying a higher voltage induces a higher current spike that relates back to a higher electro-optic coefficient in the polymer when all other parameters such as electrode area, film thickness, and processing of each layer are constant. Any changes in these parameters directly affect the variables and amount of current that will pass through the device as seen in Equation (3.2).

Chapter 4

Fabrication and Poling Results

Increasing yield during fabrication is key in real world application as is increasing the number of samples during testing. Device fabrication has multiple factors that affect the yield of polymer waveguides such as photoresist development, etch depth, imperfections, and roughness. Optimizing device processing parameters minimizes the impact of fabrication factors thus increasing yield. During the poling process of multi-layer devices the required use of high voltage puts samples at risk of dielectric breakdown and, therefore substantial damage. A large top electrode provides further increase in potential of dielectric breakdown caused by localized destructive current near pinhole defects [37].

4.1 Device Yield

The preparation of the sample is just as important as the poling process described in Section 3.4. Sample parameters such as polymer layer thicknesses and electrode surface area are defined in the design and fabrication steps. Consideration during design and fabrication can mean a lower voltage required, more efficient poling, mitigation of dielectric breakdown/flash over, and a higher yield.

There are many design parameters that need to be adheared to during fabrication of the sample for successful electro-optic poling. Failure to prepare the sample properly is detrimental to poling and the survivability of the device [16].

4.1.1 Linear Poling Realationship

The electro-optic coefficient is linearly proportional to the applied poling voltage on the EO polymer [27, 34]. Research performed by Teng and Man is shown in Figure 4.1 indicating a lower voltage can be applied to the sample during the poling process while still allowing for a large resultant electro-optic coefficient. This is advantageous as using high voltage during poling has the potential to destroy samples through dielectric breakdown.

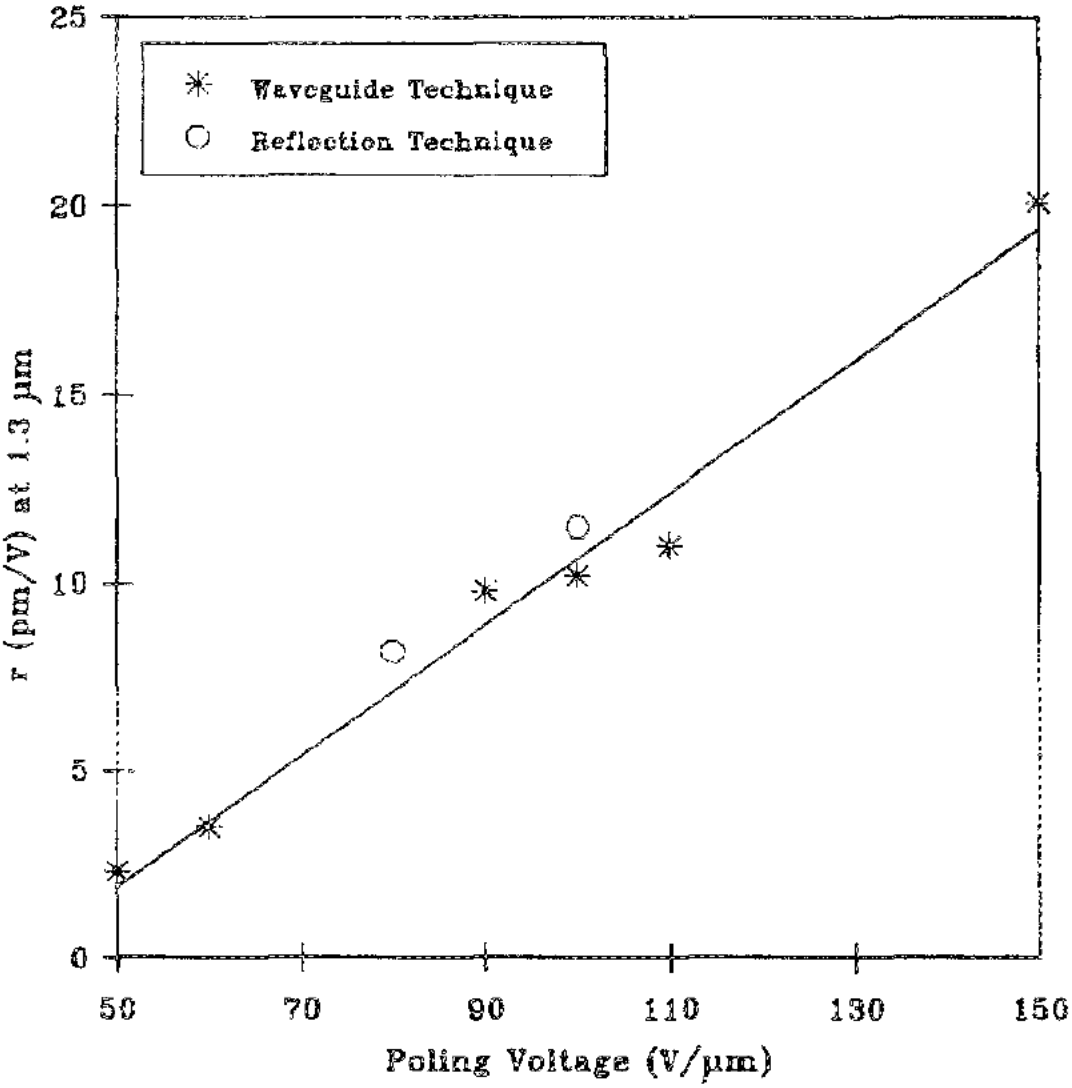

Figure 4.1: Linear electro-optic coefficient of HCC-1232 EO polymer with applied poling voltage [34]

4.1.2 Material Choice and Preparation

Material choice of core, cladding, and the substrate have cascading effects through the fabrication process. The material and design are chosen to optimize waveguide resolution, propagation loss, electro-optic coefficients, repeatably fabrication, and poling efficiency. The cost of Soluxra materials influenced the use of a polycarbonate substitute for testing parameters of the devices in the proceeding sections. The polycarbonate substitute has similar processing characteristics as Soluxra materials without the electro-optic coefficient and difference in index of refraction.

4.1.3 Layer Thickness

The thickness of each layer has a strong impact on how much voltage is needed during poling as seen in Section 3.3.2. The dimensions of the waveguide core and cladding help define single and multimode propagation along with propagation losses. These thicknesses are designed for the application and for the most part are restricted by material properties and fabrication/testing capabilities. By minimizing the thickness of the cladding layers, or increasing the thickness of the core layer, a larger portion of the electric field would be applied to the EO polymer.

4.1.4 End Face Dicing

Coupling or insertion losses of polymer waveguide devices are heavily affected by end face quality [47]. Dicing end faces of devices has the potential to reduce insertion losses during testing. The dicing blade's bond type, mesh, diamond size, spindle speed, cut speed, and the device substrates are all variables that affect the end face quality. The two device substrates tested were silicon and copper plated FR4 which defines other parameters. A Model 1100 Micro Dicing Saw was used with a THHA54060 blade for silicon and a RESR103011 blade was used for copper plated FR4 from Semicon Tools Inc.

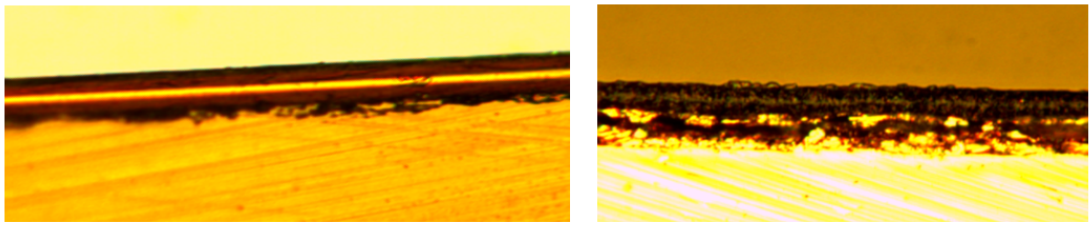

Figure 4.2: Dicing silicon (left) dicing copper plated FR4 (right)

While dicing silicon a 5 micron diamond nickel bonded blade with 40,000 rpm spindle speed and a cut speed of 100 mils/s is used to reduce delamination and give good cut quality. Reducing the spindle and cut speeds has the potential to increase end face quality, but increases the chances of the thin film polymer layers delaminating. Dicing copper plated FR4 is a less common process and required changing variables

in dicing. When using a THHA54060 blade on copper plated FR4 their is micro-delamination and layers become indistinguishable. A 30 micron diamond resin blade with 30,000 rpm spindle speed and a cut speed of 100 mils/s is used for a suitable end face quality. Sample end face quality is shown in Figure 4.2 of silicon and copper plated FR4. Use of these parameters with this blade shortened its life to just a few cuts, but offer usable end faces.

4.1.5 Flash Over Damage

The vertical separation of gold layers of approximately 15 μm at the dicing boundaries resulted in flash over in initial poling attempts at voltages below 100 V. The lack of insulation was a critical design flaw and was fixed early on in fabrication. A null horizontal barrier between the top and bottom electrodes shown in Figure 4.3 was used to remove potential for flash over at the edges of the device. A one millimeter barrier was chosen to prevent dielectric breakdown evident in Figures 3.10 and 3.11. This includes the barrier between the top electrode and dicing cut lines on all edges of the device. Since the entire bottom of the device is electrically conductive the potential of voltages in the required order of magnitude can be used.

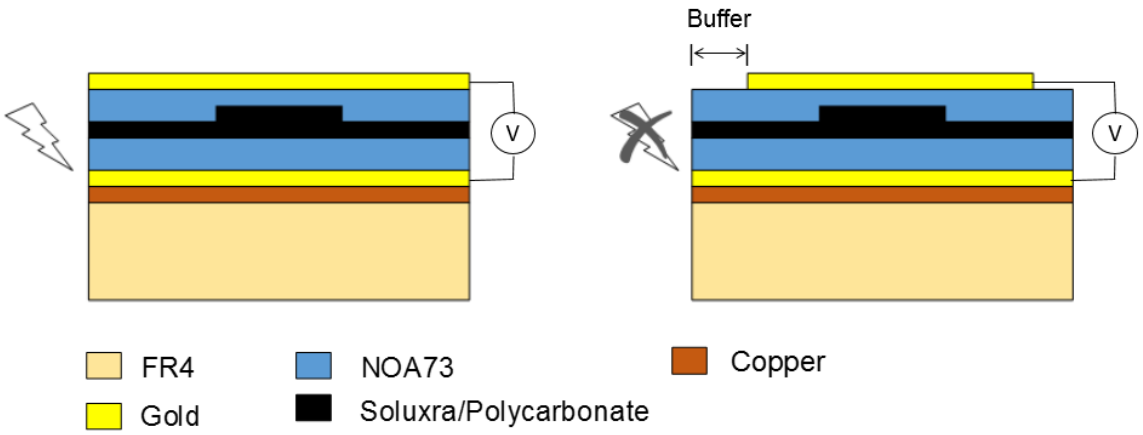

Figure 4.3: Flash over of occurring without horizontal barrier (left) No flash over with horizontal barrier (right)

4.1.6 Top Electrode Deposition

Top electrode deposition has the ability to cause formations of pinhole defects in the film which in turn causes dielectric breakdown at the location of the defect. Two methods for top electrode deposition have been studied for their impact on formation of pinhole defects that effect the maximum poling voltage. The first method is sputtering the top electrode onto the multi-layer device. Sputtering involves ejecting material in a vacuum chamber toward the device using ionized gas and heat. The second method is electron beam deposition of chrome and gold. Electron beam deposition involves high energy electrons bombarding the depositing material under vacuum. The resulting material is released from its bulk form toward the device on which it is to be deposited. The high energy required for deposition was a concern as

the depositing material could have the potential to impact the device and drive into subsequent layers to create pinhole defects.

Table 4.1
Max voltage test for poling radial bends made from polycarbonate as a core layer substitute. All electrodes are sputtered with chrome and gold

Max Sustainable Voltage	**Silver Epoxy**	**Damage Description**
400 V	✓	Major imperfection
400 V	✓	Minor imperfection
600 V	X	Layer peeling off
600 V	X	Minor imperfection
900 V	✓	Major imperfection
1600+ V	X	Minor imperfection
1600+ V	X	Minor imperfection

Maximum voltages applied before dielectric breakdown occurred while testing for sputtered electrodes and are tabularized in Tables 4.1 and 4.2. The damage descriptions refer to the state of the device before poling, as fabrication handling and processing is not perfect. Silver epoxy was used in Table 4.1 to test its ability to mitigate defects based on probe contact. The silver epoxy caused the the devices to fail at lower voltages compared to just using the probes. Comparing Tables 4.1 and 4.2, there are insignificant differences in the maximum sustainable voltage for

sputtering or electron beam deposition of the top electrode in device fabrication.

Table 4.2
Max voltage test for poling radial bends made from polycarbonate as a core layer substitute. Top electrodes are electron-beamed while bottom electrodes are sputtered with chrome and gold

Max Sustainable Voltage	**Damage Description**
200 V	Major imperfection
300 V	Minor imperfection
500 V	Minor imperfection
600 V	Minor imperfection
1400 V	Minor imperfection
1600+ V	Layer peeling off
1600+ V	Minor imperfection
1600+ V	Minor imperfection

4.1.7 Maximum Sustainable Voltage and Top Electrode Deposition

Because of damage during poling at high electric fields the need to decrease the amount of voltage applied to samples became relevant to increase sample yield [48]. Complete structures of radial bends were fabricated with polycarbonate to test for

maximum threshold voltage before dielectric breakdown. Minor surface conditions and imperfections were noted from processing. Efforts to reduce these imperfections were addressed in fabrication. The difficulty is that the radial bends have a large pad area of 9 cm^2. Silver epoxy was applied to the top of the gold electrodes on three samples for performance testing.

Table 4.2 indicates that the use of sliver epoxy with probes lowers the damage threshold voltage of samples. This is most notable with the sample with no damage being only able to sustain 400 V before damage from sparking occurred. All samples survived at 400 V, hence this is a good baseline for future poling of radial bends. By using probes with no silver epoxy and a voltage at 400 V yield from poling is increased while still increasing the electro-optic coefficient outlined in Section 4.1.1.

4.2 SEO100C Refractive Index Changes from Poling

Refractive index measurements of the limited SEO100C samples on ITO glass were taken from the prism coupler were taken . Extreme caution was taken while measuring these samples during the poling process as to not damage them due to dielectric breakdown. Additional tests were conducted on the samples to determine their electro-optic coefficient's ability to withstand processing conditions.

4.2.1 Step Index After Poling

Electro-optic poling induces chromophore dipoles to become permanently fixed in alignment with an applied electric field as described in Section 3.1 . The alignment creates a step change in index of refraction of the material, in addition to the increase in electro-optic coefficient [36]. The strength of the applied voltage field determines the efficiency of alignment which is related to the magnitude of the index step change along with the electro-optic coefficient [27, 36, 38].

Index of refraction results from poled and non-poled SEO100C from the prism coupler are displayed in Tables 4.3 and 4.4. The final poled n values cannot be compared to cited values of index, as they are measured at a wavelength of 1543 nm. Each thin film sample was poled at 100 V and the V/μm was calculated by dividing 100 V by the measured thickness of each film from the prism coupler.

Table 4.3
TM refractive index of SEO100C measured by prism coupler

	Non-Poled	**Poled**	**Δ (10^{-3})**
Sample 1 (39 V/μm)	1.64592	1.64994	4.02
Sample 2 (44 V/μm)	1.64794	1.65272	4.78
Sample 3 (51 V/μm)	1.65215	1.65701	4.86

Table 4.4
TE refractive index of SEO100C measured by prism coupler

	Non-Poled	**Poled**	**Δ (10^{-3})**
Sample 1 (39 V/μm)	1.66343	1.66148	-1.95
Sample 2 (44 V/μm)	1.66390	1.66236	-1.54
Sample 3 (51 V/μm)	1.66526	1.66159	-3.67

The TM index of refraction is of primary concern as it relates to the r_{33} coefficient increase. A TM step index increase of 0.00402-0.00486 TM index with voltages of 39-51 V/μm is seen from Table 4.3 per 100 V/μm. The step change is expected to be linear with respect to the applied electric field but was not observed. Three samples it is not enough to show this relationship due to allowances for errors in measurement of index and thickness.

4.2.2 Mid-Process Poling

Mid-process poling can be used to help increase electro-optic poling efficiency of the thin films. It has been shown that cladding material with high resistivity compared to the core negatively effects the electro-optic coefficient after being poled because of the high voltages used as outlined in Section 3.3.2 [39]. Conducting electro-optic

poling before the top cladding layer is applied to a device has the potential to significantly reduce the need for high voltages near the dielectric breakdown point while maintaining a large increase in electro-optic coefficient. Fabrication conditions after spinning the EO polymer layer, such as hot plate temperatures and etching environments, were used to test possible changes in the n step change of the thin films from Section 4.2.1.

4.2.2.1 Reduction of Voltage

By pausing fabrication and poling a partial stacked device, a lower voltage can be used for the same increase in electro-optic coefficient. This greatly reduces the possibility of dielectric breakdown of the device due to the lower voltages used.

Based off of Equation (3.2) and a partially stacked layer consisting of a bottom and top electrode, one 4.5 μm layer of NOA73, and a 3.4 μm layer of un-etched Soluxra SEO100C Table 4.5 shows a reduction of dielectric breakdown while ensuring high poling efficiency.

Table 4.5
Voltage difference based on mid-fabrication versus post fabrication poling based on Equation (3.2)

V/μm on Core	**Full Stack Voltage**	**Partial Stack Voltage**
25	333 V	209 V
50	665 V	418 V
75	998 V	626 V
100	1330 V	835 V

The removal of one of the cladding layers does decrease the protection that the EO polymer has from the poling process, but the use of 63% less voltage compared to the full stack balances out the disadvantages. Another advantage to this method is that the EO polymer is at a uniform thickness compared to poling after etching occurs. After etching there are waveguides present that alter the thickness of the core material and therefore the electric field applied locally to the polymer. There is concern with uniform poling the regions with waveguides and this non-uniform thickness provides a path of lower resistance for electrical charge and increases the potential for dielectric breakdown.

4.2.2.2 Index Change

In order to investigate the possibility of mid-process poling, samples from Section 4.2.1 underwent processing conditions. Because of the temperature and exposure experienced by the device during processing it could be possible for the chromophore dipoles to relax to their original random orientation. Sample 3 in Table 4.6 was damaged due to cracking in the glass layer and TM polarization and was unable to be measured.

Table 4.6
TM refractive index change from poled SEO100C samples after additional processing

	UV Exposure	**120°C Bake**	**Etch**	**Δ (10^{-3})**
Sample 1 (39 V/μm)	X	✓	X	-0.70
Sample 2 (44 V/μm)	✓	✓	✓	-0.75
Sample 3 (51 V/μm)	✓	X	X	N/A
Average 120°C Bake				-0.72

Refractive index of TM dropped 16% due to baking on a hotplate for 2 hours at 120°C. This is a good first study to determine if Soluxra can retain its electro-optic coefficient while being poled mid-processing. The advantage of this is a larger increase in r_{33} while applying the same voltage level to the partial stack compared to the fully

fabricated device. If 400 V is applied to the sample while poling with one layer of NOA73 and SEO100C and thicknesses from Section 3.3.2 the poling field can be increased across the core from 30 V/μm to 48 V/μm. With this higher electric field, and taking into account a 16% relaxation in electro-optic coefficient, the poling efficiency can increase to 43% of the recommended 100 V/μm compared to 30%.

Table 4.7
TE refractive index change from poled SEO100C samples after additional processing

	UV Exposure	**120°C Bake**	**Etch**	**Δ (10^{-3})**
Sample 1 (39 V/μm)	X	✓	X	-2.14
Sample 2 (44 V/μm)	✓	✓	✓	-3.32
Sample 3 (51 V/μm)	✓	X	X	0.008
Average 120°C Bake				-2.73

The TE index of refraction is of little concern to the fabricated devices, but it is something to monitor. The TE index had insignificant change from 30 minutes of UV curing. Also notable is that fact that this index continued to decrease with the 120°C baking required for driving solvents out of the top NOA73 cladding layer.

4.3 Alternative Electro-Optic Polymers

One main issue with the poling studies has been the scarcity and cost of SEO100C. Switching to a cheaper EO material that is commercially available would allow for more complete tests through poling. Materials such as DR-1 PMMA can be used as an EO polymer substitute [38, 43] . Initially the DR-1 PMMA fabrication of thin films resulted in high density pinhole defects causing electrical shorts.

During material choice SEO100C was chosen due to its high electro-optic coefficient potential and the ability to spin coat thin layers without electrical shorts. There are documented papers about successful device fabrication using SEO100C [20, 42].

Using such materials would mean adjustment to fabrication process parameters. Major concerns faced in the fabrication include delamination of the stacked layers from the substrate during dicing, consistent photolithography techniques, and reaching the appropriate etch depth for singlemode waveguides. With these cheaper materials a smaller yield is acceptable and more testing can be done with higher sample numbers.

DR1-PMMA can be used as one of these low cost EO polymers [43]. T_g for DR1-PMMA is approximately 130°C based on weight percentage and has shown r_{33} values of up to 32 pm/V after poling [43]. These modest values match closely with $LiNbO_3$, but with the DR1-PMMA polymer advantages outlined in Section 1.3 are applicable.

Chapter 5

Mach-Zehnder Coupling and Testing

For modulation as an MZI the half-wave voltage (V_π) can be measured to determine the r_{33}. Applicable devices include Mach-Zehnders and ring resonators that use a reference beam for interference. This can be achieved in a laboratory setting where active coupling alignment is performed with tapered fibers. Figure 5.1 shows active coupling of a MZI essential for measurement of r_{33}.

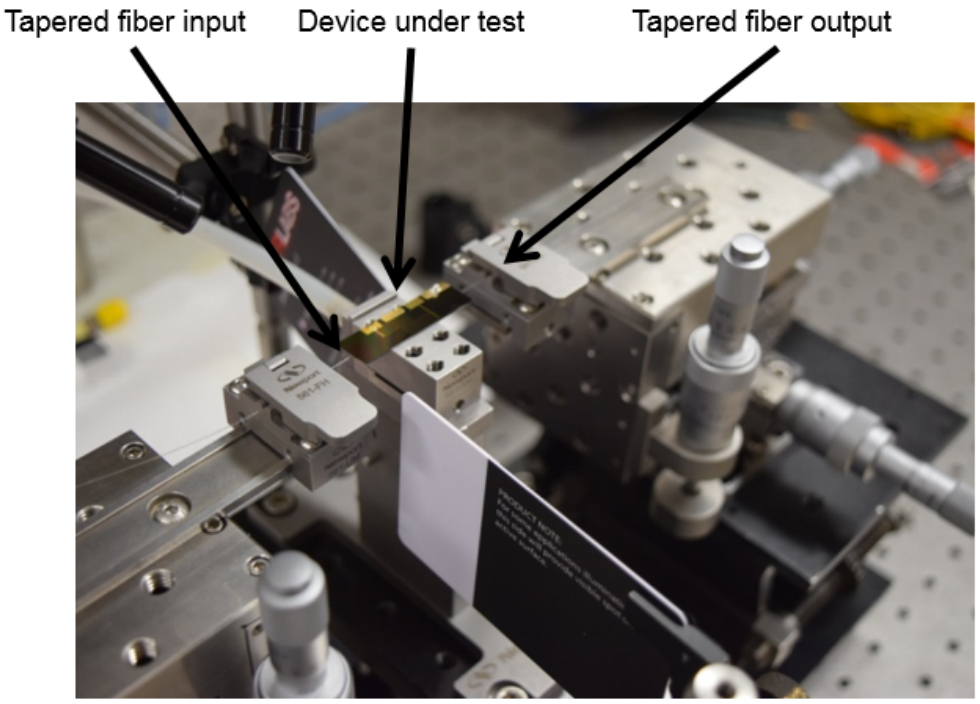

Figure 5.1: Tapered Fiber Coupling used for V_π and two-tone measurements

TM polarization is launched into the device and a DC voltage applied to its electrodes. The voltage is increased and power measurements are taken at the output. V_π can be measured using the voltage difference between maximum and minimum power values. Intermodulation distortion (IMD) can be measured in devices as well by performing a two-tone test [49]. A tabularized list of equipment used for measurement of fabricated and commercially purchased devices in the lab is in Table 5.1.

Table 5.1
Table of equipment used for measurement

Equipment Description	**Manufacturer/Model(s)**
RF Signal Generators	Keysight/HP E8257C/83620B
RF Isolators	RF Lambda 0.7-1, 2-6 GHz
RF Amplifiers	Mini-Circuits ZJL-6G+
RF Low Pass Filters	Mini-Circuits VLF-3000+ VLF-5500+
RF Combiners/Splitters	RF Lambda 0.5-2, 2-8 GHz
RF Attenuator/Driver	Agilent M11713B/8494H-002/849
High Power Laser	Gooch & Housego EM650
Wavelength Tunable Laser	Ando AQ4321A
Optical Attenuators	Thorlabs FAK05
Optical Polarization Controller	Thorlabs FPC652
Fiber Alignment Stages	Newport x-y-z 562 Series
Tapered Fibers	OZ TPMJ-3A-1550-8/125-0.25-7-2.5-14-2
Optical Power Detector	Newport 818-IR
Optical Linear Polarizer	Thorlabs LPIREA100-C
PIN Photodetectors	Optilabs PD-20M
DC Power Supply	Agilent E3646A
Spectrum Analyzer	Rhode-Schwartz Z & L
Optical Spectrum Analyzer	Ando AQ6317B

A commercial modulator was purchased for lab configuration verification and comparison testing in Figure 5.2. The MXAN-LN-10 Mach-Zehnder modulator from Photline operates at 1550 nm with an RF bandwidth from DC-12 GHz. Using the commercial modulator the half-wave voltage response and the two-tone test necessary for obtaining the IMD was performed. The modulator had FC/ACP optical connectors and an SMA RF connection to easily integrate into the test setup.

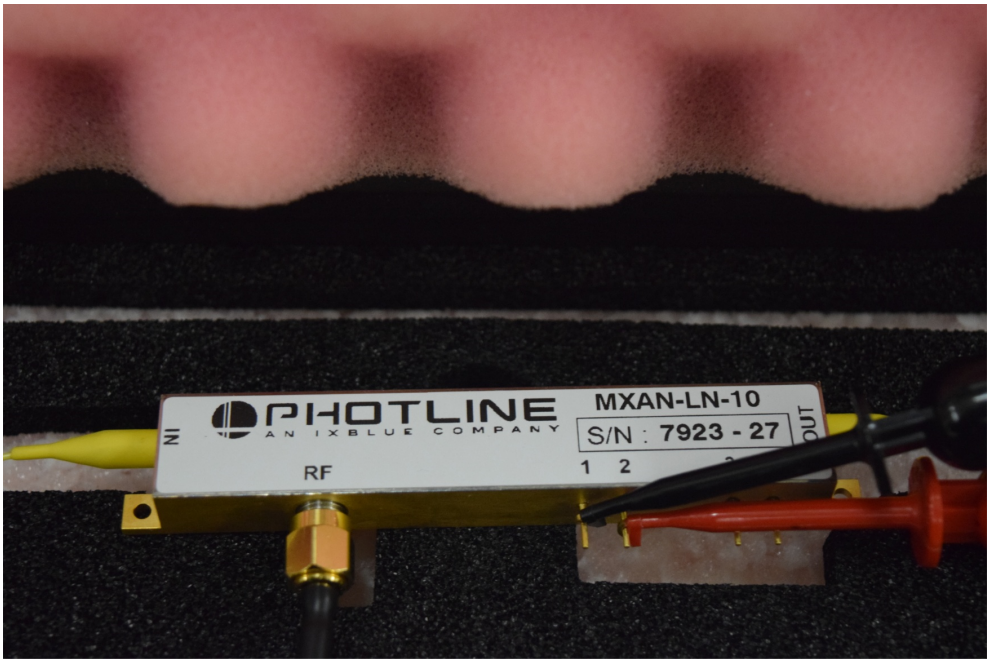

Figure 5.2: Photline MXAN-LN-10 with optical, RF and DC voltage applied

EO polymer devices have not been available for testing of their V_π due to fabrication difficulties and a limited supply of SEO100C. The measurement setup has been verified using the commercial Photline MXAN-LN-10 and can be used to calculate the r_{33} coefficient of the EO polymers from Equation (2.5) in fabricated devices.

5.1 Voltage Bias (Half-Wave Voltage)

The half-wave voltage (V_π) measurement is used for characterization of multi-layer devices. The half-wave voltage is described in Section 2.3.1 and is defined by Equation 2.5 for MZIs. The phase changes induced by the EO polymer waveguide from the voltage bias allow for constructive and deconstructive interference at the output.

5.1.1 Measurement Procedure

Measurement of the V_π requires coupling light into the waveguide and measuring the output power based on changes in the bias voltage. A flowchart of the measurement process is provided in Figure 5.3. The laser is TM polarized from the polarization controller because the TM polarized light by the phase shift based on geometry. A tapered fiber like the one seen in Figure 5.4 is used to couple light into the device.

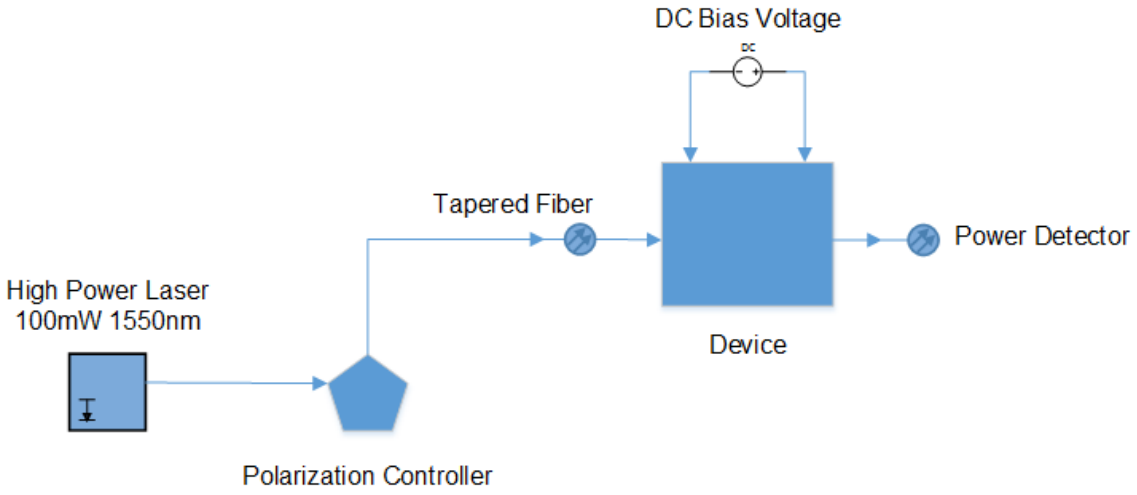

Figure 5.3: Measurement procedure for half-wave voltage

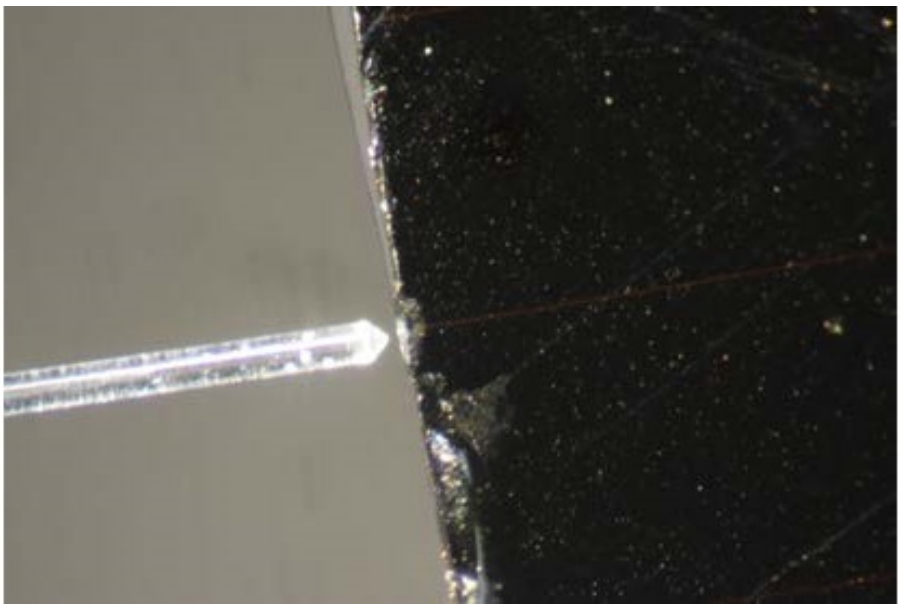

Figure 5.4: Tapered fiber coupled into a fabricated waveguide

5.1.2 Measurement Setup

The laser used for the experimentation is a Gooch & Housego EM650 100 mW distributed feedback (DFB) laser working at 1550 nm with polarization maintaining fiber. The polarization of the laser was measured using a rotating linear polarizer and a power meter. From Figure 5.5 it can be seen that the laser is polarized at 38.9° from the vertical. This is a mixture of TE and TM modes. For measurement only the TM mode needs to be excited and therefore the laser output needs polarization manipulation. To isolate the TM polarization a Thorlabs FPC562 manual polarization controller is used with three 56 mm radius fiber paddles. TM polarization is determined by using an objective lens to collimate the beam into a linear polarizer with the transmission axis set at 0° and into a power detector. This allows for the paddles to be configured until the maximum power is seen while the polarizer is set to 0 degrees from vertical seen in Figure 5.6. If pressure is applied to the fiber, is moved, or temperature is changed significantly, the polarization will be changed and TE will also propagate. This is mitigated by using polarization maintaining patch cords after polarization is set and fixing all fibers. With the TE polarization extinguished the tapered fiber can be coupled to the device.

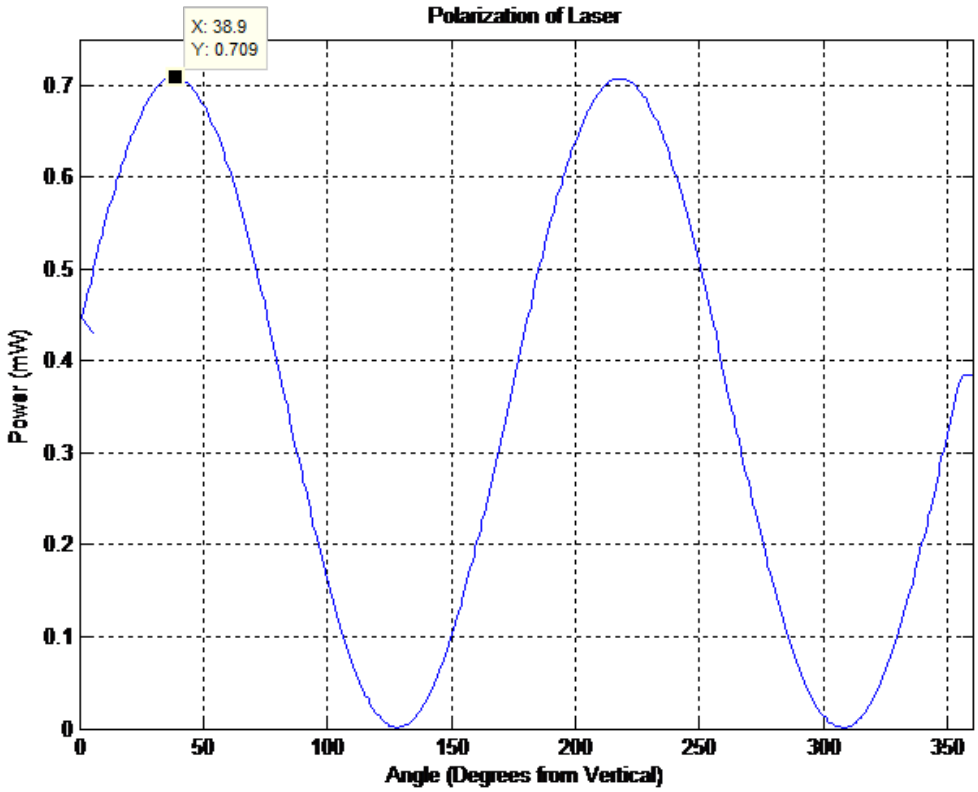

Figure 5.5: Polarization of EM650 high power laser at 38.9° from vertical

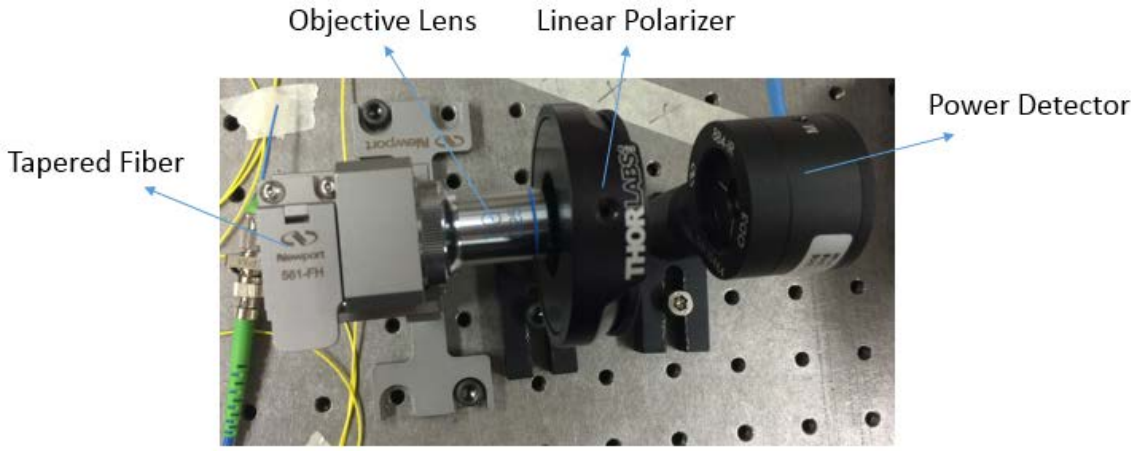

Figure 5.6: Setup for determining polarization output from a tapered fiber

The laser can be connected to a variable attenuator or fixed attenuators for precise control over power before the manual polarizer. Polarized light is then transferred to an OZ polarization maintaining tapered fiber. The OZ tapered fiber has the specifications outlined in Table 5.2. The output of the device is collimated using a 10x objective lens to the Newport power detector in Figure 5.7. A DC voltage supply is applied to the device and varied while monitoring the power to determine the V_π.

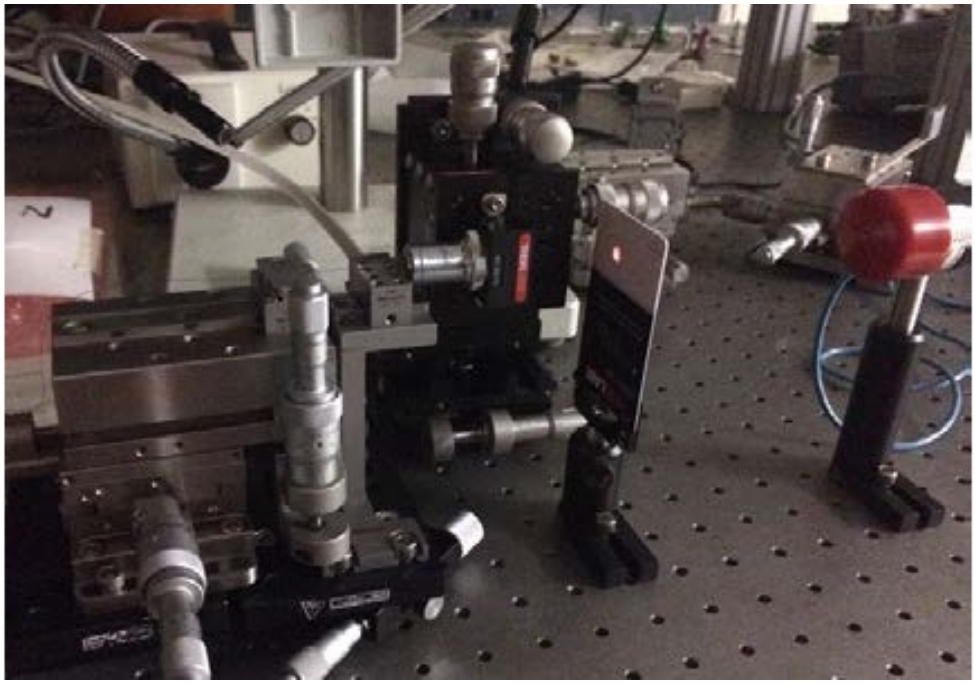

Figure 5.7: Collimation of light for power measurements

Table 5.2
OZ tapered fiber specifications

Length	2 m
Wavelength Operation	1550 nm
Jacket	OD 0.25 mm 8/125 μm
Polarization Maintaining	✓
Connectors	FC/APC & Tapered Tip
Stripped Length	7 mm
Spot Diameter	2.5± 0.5 μm
Working Distance	14± 2 μm

5.1.3 Commerical Mach-Zehnder Results

Using the FC/ACP optical fiber connectors the 1550 nm high power laser was coupled into the commercial modulator and outputted to an IR power detector. An SMA connector was used for an RF signal to be input into the modulator and leads were clipped to a DC voltage supply to apply the bias voltage. From Figure 5.8 the V_π was measured to be 6.4 V for the Photline MXAN-LN-10. This value is found by finding the applied voltage at which there is a phase shift of π. Such a phase shift implies going from completely constructive interference to completely destructive interference.

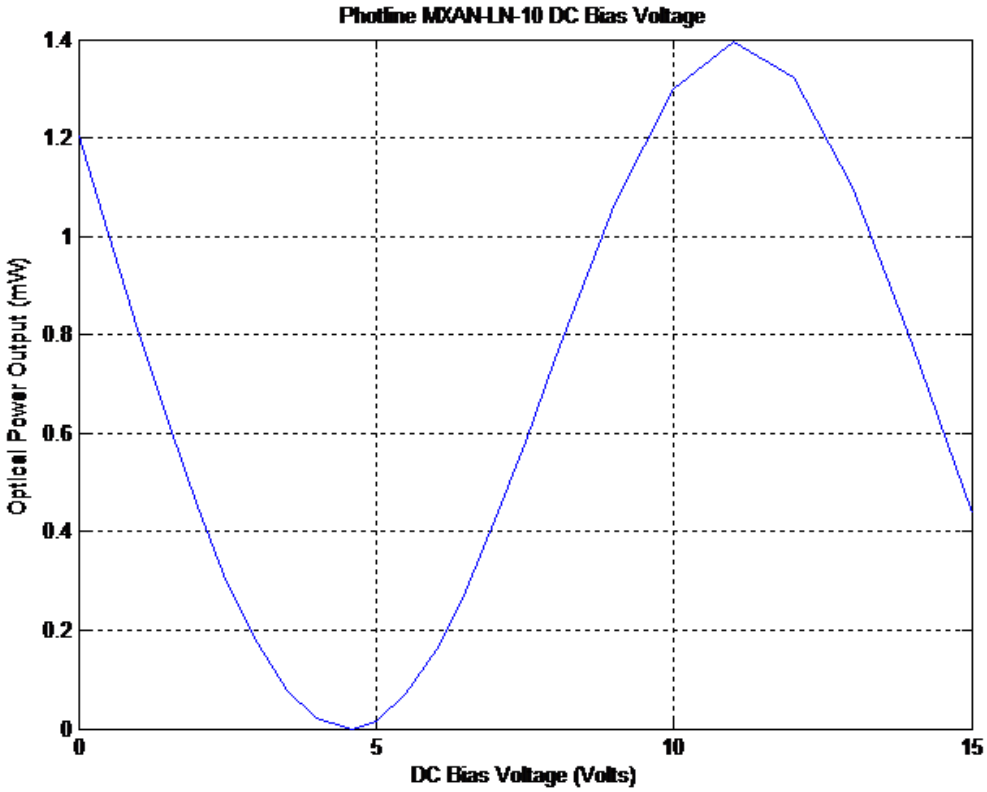

Figure 5.8: DC bias voltage response from Photline MXAN-LN-10 modulator

5.2 Two-Tone Test

The laboratory configuration is also capable of measuring IMD and spurious-free dynamic range (SFDR) using the setup in Figure 5.9 [50]. Two signals separated by a small frequency are generated and combined with isolators, amplifiers, attenuators, and combiners for input into a modulator. When the signal is extracted from the light after modulation using a photodetector, the signal is analyzed for third order IMD.

SFDR follows from the IMD measurements [3, 12, 50, 51, 52]. These measurements are important for device characterization. Future fabricated devices will be able to use these test setups to validate their designs.

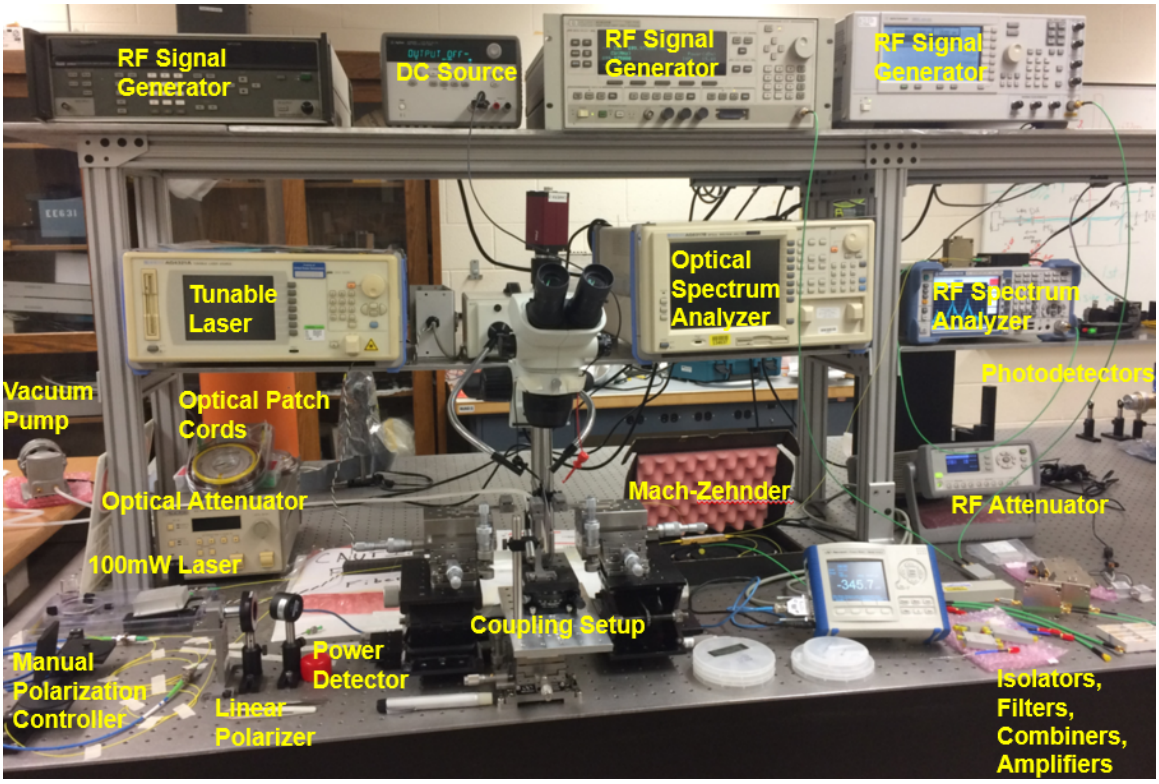

Figure 5.9: Device testing lab used for V_π and two-tone measurements

The two-tone test involves sending two different frequency signals through a device. The frequency separation is close enough to cause intermodulation interference. This interference produces signals in the side bands of the original signals and therefore distorts any other signals that might be present in those side bands. It is largely important in communication as it will limit the capacity of signals that can be sent within a channel bandwidth.

The third order IMD side bands of interest are in close proximity to the fundamental signals. Even order IMD pulses are spectrally far enough away to be ignored along with the harmonics that can be filtered out. The distance and strength depends on the frequency separation of the original signals. When more than two signals are sent through the channel, these IMD products will overlay on the fundamental signals causing interference. This could mean that power needs to be increased to overcome the noise, the frequency separation between fundamental signals need to increase, or a combination of the two.

5.2.1 Measurement Procedure

The two-tone measurement is more involved than the half-wave voltage. The flowchart in Figure 5.10 shows signal propagation through the test setup. Isolators, amplifiers, and attenuators are used to control the power of the signals through each component and to prevent reflected power that can damage components.

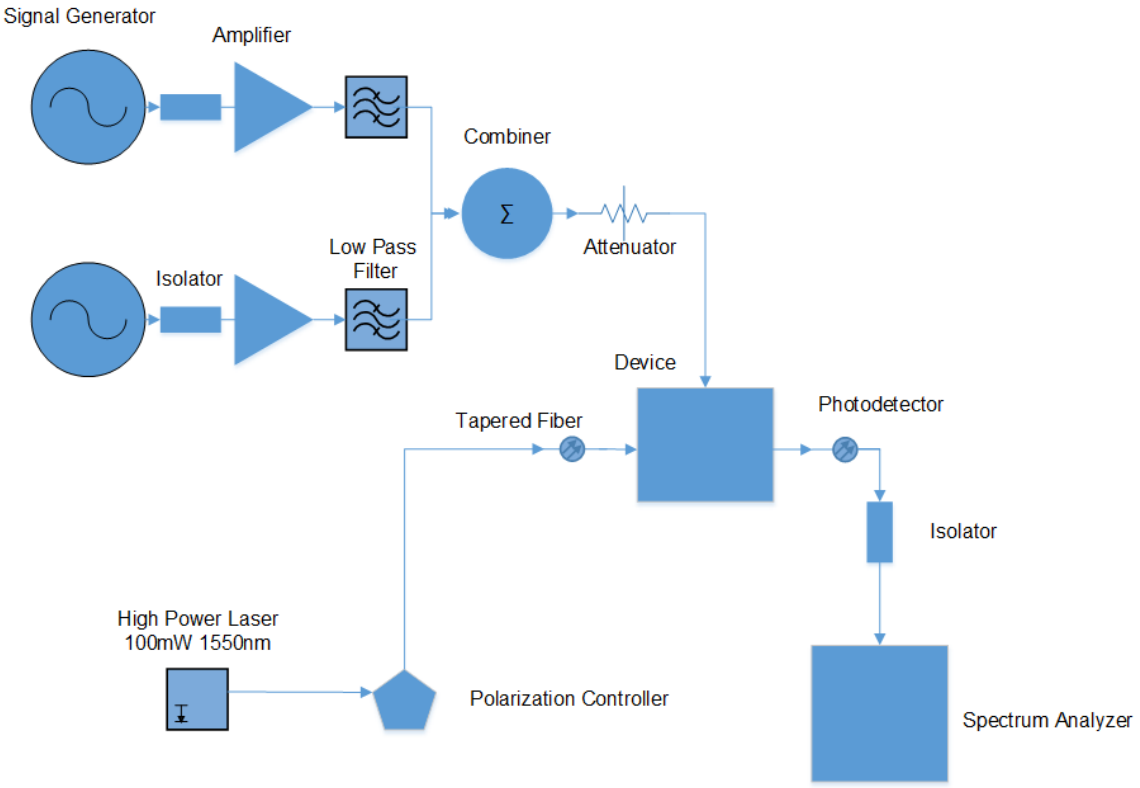

Figure 5.10: Flowchart of two-tone testing

5.2.2 Measurement Setup

Coupling of the laser is similar to the half-wave voltage measurement in Section 5.1.2. The main difference is that the output signal needs to be coupled into another fiber to propagate to a photodetector. Once at the photodetector, the signal is demodulated and the IMD is measured. The laboratory configuration can be seen in Figure 5.9.

5.2.3 Commerical Mach-Zehnder Results

Connection of the Photline MXAN-LN-10 was similar to the description in Section 5.1.3 with the exception of the output FC/ACP optical fiber end connected to a photodetector for demodulation. The IMD was measured using the two-tone test setup with a 50 kHz frequency separation centered at 900 MHz as 28 dBm in Figure 5.11. To measure the IMD the height of the fundamental frequencies are subtracted from the third order side bands [49, 51, 53]. There are third order IMD side bands at $2f_2 - f_1$ (900.075 MHz) and $2f_1 - f_2$ (899.925 MHz) from the fundamental signals. This data serves as a standard for which fabricated modulators will be compared along with ensuring that the test setup works properly before fabrication of the modulators are complete.

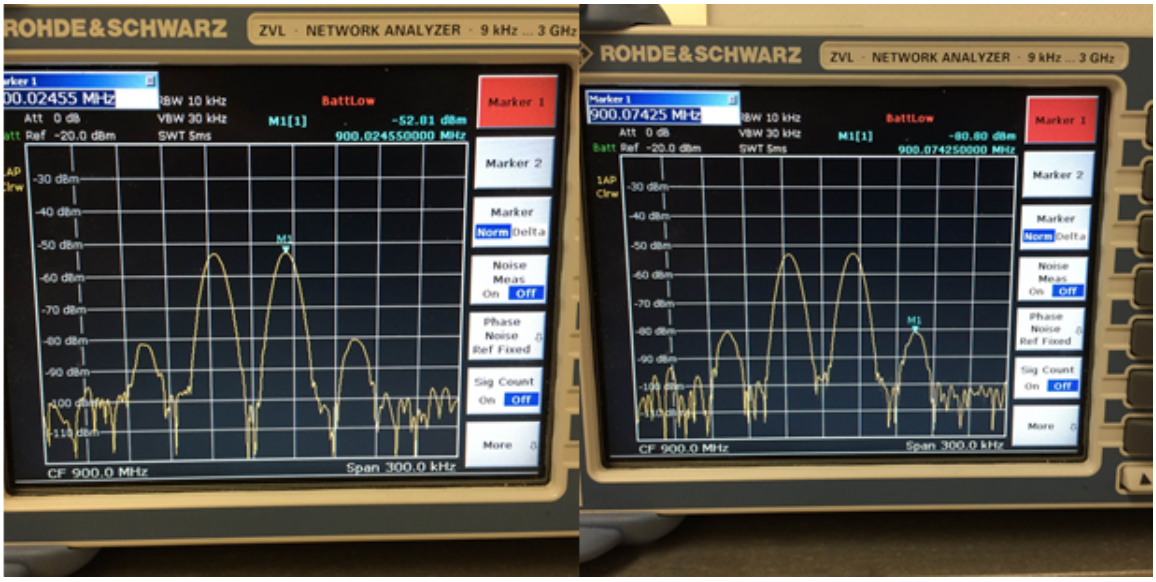

Figure 5.11: Two-tone test of Photline MXAN-LN-10 with 50 kHz frequency separation centered at 900 MHz with an IMD of 28 dBm

5.3 Fabricated Mach-Zehnder

Fabricated devices are tested against the commercial Mach-Zehnder. Coupling into the waveguides presented its own challenges as it is difficult for the power to be stable at powers under 100 μW. Losses in coupling and propagation reside in fabricated polymer waveguide devices.

5.3.1 End Face Damage

Coupling and testing of the device is problematic with high insertion and propagation losses of EO polymer waveguides as high input power is used to overcome these losses. With the combination of using tapered fibers and a high power laser source damage at the end faces occurred while testing device metrics due to high laser irradiance. Power at the output of the first OZ tapered fiber was measured to be 56.6 mW. The two micron spot size can produce an irradiance of about 1.8 MW/cm_2 at the measured power 56.6 mW with a minimum spot size of 2 μm.

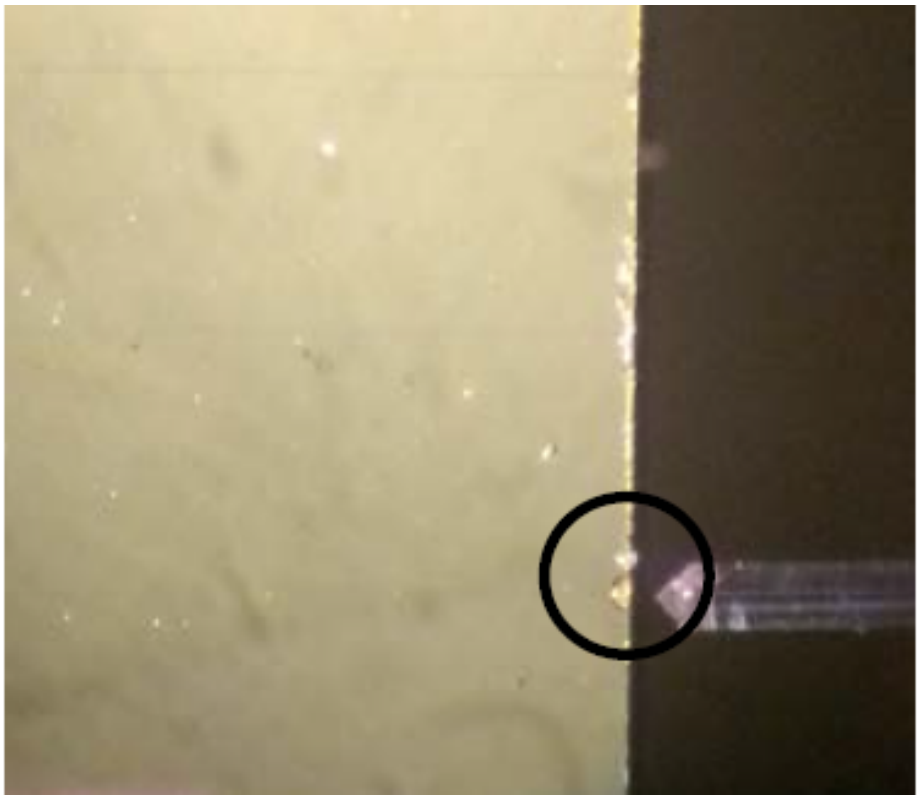

Figure 5.12: Top damage from laser coupling

Damage at the end face was observed during coupling of the device from the top view seen in Figure 5.12. Minor flashes of light were observed when the device was brought near the focal point of the tapered fiber. The large irradiances are well beyond the damage threshold of the polymer layers. Damage observed under a microscope in Figure 5.13 shows complete removal of the layers and damage to the substrate. An attenuator is connected behind the manual polarization controller to prevent scorching of the polymer material and reducing the power level to below 25 mW where no damage was observed.

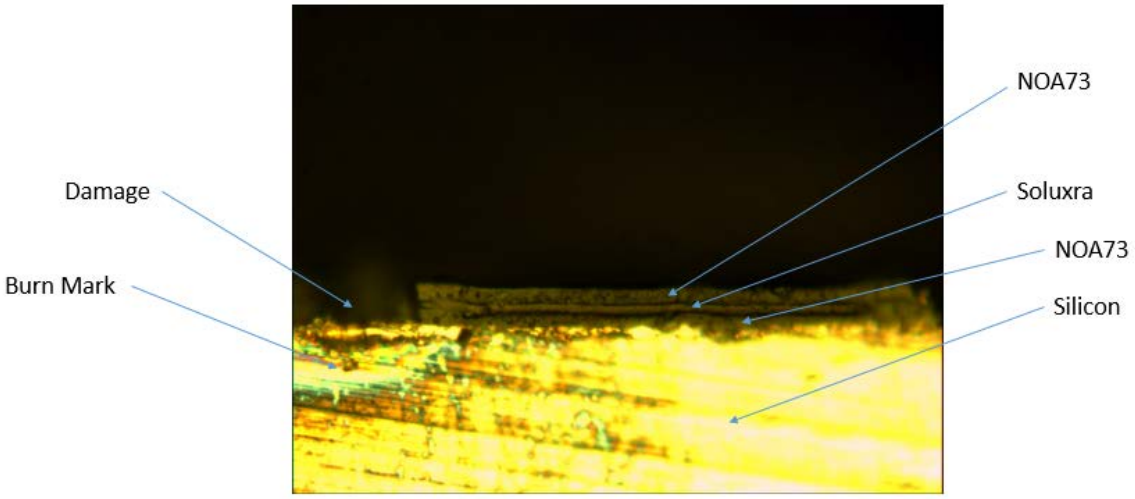

Figure 5.13: End face damage from laser coupling

5.3.2 Measurement Setup

Measurement setup of fabricated devices focuses on coupling of light as the electrical inputs to the device have been validated using the commercial modulator. Coupling into the waveguides presented its own challenge as it is difficult for the power to remain stable at powers under 100 μW. Figure 5.14 shows coupling into the waveguides onto a camera and Figure 5.15 shows coupling onto an IR detection card.

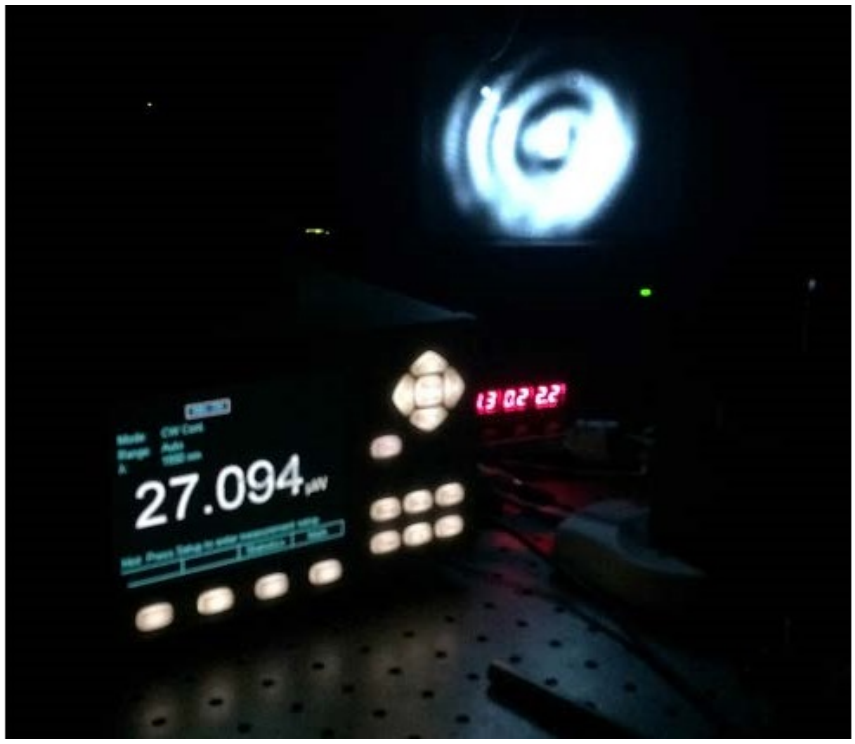

Figure 5.14: Profile of light at output of Mach-Zehnder and collimated

Figure 5.15: Profile of light at output of Mach-Zehnder on infrared detection cards

Parameters to quantify the device are the insertion and absorption losses. These losses are currently a major issue in EO polymer devices and need to be addressed. A plan was put in place to use the cut back method to measure these values in straight waveguides with the same fabrication steps. The issue is that coupling of light into the waveguides produce multiple propagating beams along with a large amount of power in the cladding layer. The typical output produces a bar of light seen in Figure 5.15 with between 3 and 6 distinguishable bright dots.

Chapter 6

Research Summary

Environment and fabrication procedure can affect the efficiency of poling of the EO thin film polymers. Further studies need to be carried out on thin film poling and multi-layer devices to increase r_{33} while maintaining a high yield. Materials, design, and poling setup are explored in Section 6.2.

6.1 Conclusion

Poling of polymers requires an understanding of how design, fabrication, and poling setup will affect the resultant r_{33} and yield of the device. Electro-optic contact poling and testing of Soluxra SEO100C devices and thin films was made possible through

laboratory design and configuration. The laboratory poling configuration consists of the sample mounted on a dielectric barrier in an oven with micro-manipulating probe tips that come into contact with the top and bottom electrodes of the sample. The oven is heated and cooled while a constant DC voltage is applied to the sample. Current and voltage measurements are used to monitor poling and give initial evidence of poling occurring.

To increase the yield of samples from poling, a dielectric barrier was incorporated into the design, voltage was decreased, and top electrode deposition was explored. A horizontal dielectric barrier was used between dicing lines and the top electrode to prevent flash over damage. The maximum sustainable voltages of several devices with large top electrode surface areas with varying defects were studied and the result was to 400 V for a 100% yield from poling. The effects of sputtering and electron beam deposition of the top electrode showed that there is no correlation between deposition method and maximum sustainable voltage.

Measurement of thin films and multi-layer devices are treated differently due to testing capabilities. The step change of n can be measured using a prism coupler while it has been shown that the V_π and IMD of a MZI can be measured with the laboratory configuration in Chapter 5. Initial results have been demonstrated from the constructed laboratory poling configuration of a commercial MZI for validation of poled thin film and multi-layer devices. Dicing parameters were evaluated for quality end

faces of waveguide profiles for decreased coupling losses. A TM step index increase of 0.00402-0.00486 TM index per with voltages of 39-51 V/μm with SEO100C thin film samples has been shown after poling. As a proof of concept the SEO100C thin film samples were introduced to processing conditions to mimic the effects of poling the film mid-process on multi-layer devices. After mid-processing conditions were applied, the TM step index relaxed an average of 16% back to their original values.

6.2 Future Work

The majority of scientific research continues with new or different ways of improving on the work that has already been done and the work presented in this thesis is no different. Alternative fabrication, poling, and testing procedures are explored to improve final device metrics such as poling efficiency, measurement, and consistent yield.

6.2.1 Fabrication

Fabrication steps, materials, and design of the multi-layer device impact ease of processing, poling, and testing. The design of the device might make processing easier by use of alternative materials, but at the cost of tolerances. Use of different materials

may cause fewer complications within fabrication, but may negativity affect testing and poling efficiency.

6.2.2 Low Resistivity Cladding Layers

The ability to use low resistivity cladding layers is dependent on fabrication techniques and material compatibility. The addition of cladding layers allows for indirect electrical contact with the core polymer layer. Table 6.1 shows the advantage of using a cladding layer with lower resistivity compared to the core. This is assuming a stacked device consisting of a bottom and top electrode, 4.5 μm thickness for the above and below cladding layers, and a 3.4 μm thickness of the core layer. The assumed resistivity of each material is 10^{10} Ωcm and 10^{9} Ωcm for the core and cladding material respectively.

As seen in Table 6.1 the increase of voltage from a thin film to a multi-layer device is considerably less when using cladding layers of just one order of magnitude less resistivity than the core. Use of low resistance material as cladding layers has been shown to achieve nearly 100% poling efficiency when compared to thin film poling of SEO100C material [21, 39].

Table 6.1
Voltage difference based one resistivity of the cladding material being one order of magnitude lower than the core material from Equation (3.2)

.

V/μm on Core	Voltage Applied to Core	Voltage Applied to Device
25	85 V	108 V
50	170 V	215 V
75	255 V	323 V
100	340 V	430 V

6.2.3 Inverted Rib

Two designs in fabrication are available when building slab rib waveguides. The raised rib and the inverted rib are pictured in Figure 6.1. Considerations in the choice of design of the device include chemical interactions, photolithography resolution, etching, and other unforeseen complications.

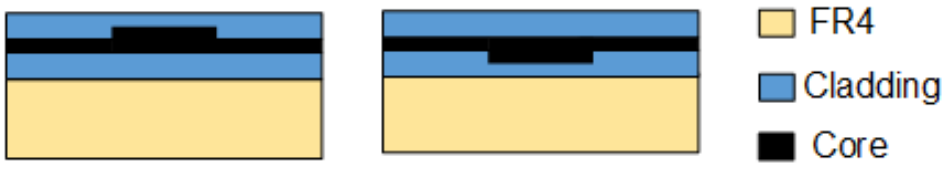

Figure 6.1: Raised rib design (left) Inverted rib design (right)

Initial work has been done to investigate fabrication design of an inverted rib design. A major difference between the raised rib and the inverted rib is that etching into the cladding layer instead of the EO polymer is required. This can be advantageous when the EO polymer has a high cost such as SEO100C because the cladding layer can be processed multiple times until the correct trench structures are made for the waveguides before applying the polymer. The EO polymer would not have to undergo any of the photolithography or etching conditions increasing the device yield.

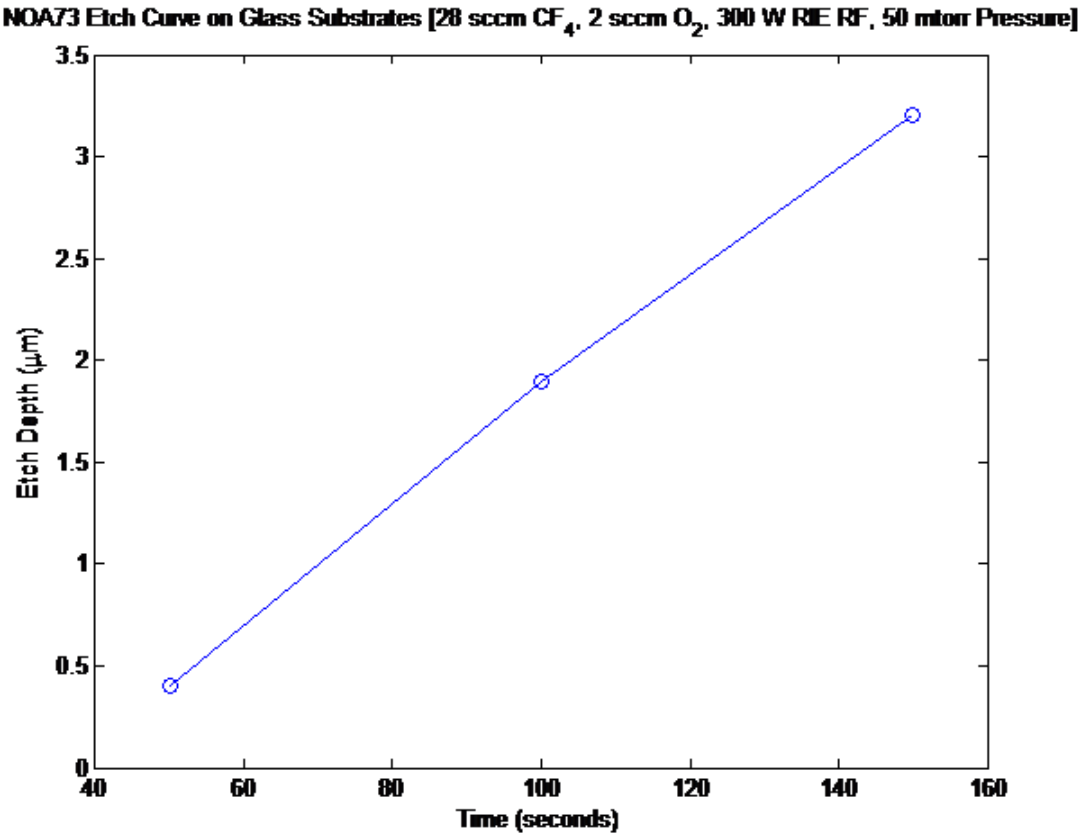

Figure 6.2: NOA73 etch curve on glass substrate. RIE etching with 28 sccm CF_4, 2 sccm O_2, 300 W RF, and 50 mtorr pressure

The cladding material needs to be etched for the inverted rib so an etch curve of NOA73 shown in Figure 6.2 was made from multiple samples spun on glass slides using appropriate fluoride gases [54]. More etch recipes need to be tested and curves created for optimal etching with NOA73 and the photoresist. NR9-1500P as a negative photoresist is compatible with the current process and masks. Photolithography parameters such as spin speeds, pre and post exposure bakes, exposure levels, and development times need to be optimized based on the substrate for desired features.

6.2.4 Roughness Characterization

Roughness of the device can have an impact on poling efficiency due to electrodes not necessarily being flat. This can cause variations in perpendicularity of the applied electric field to the EO polymer. This possible variation would align the dipoles in unwanted orientations [55].

Table 6.2
Roughness of silicon and FR4 substrates with NOA73 and polycarbonate layers

Substrate	**Average Roughness (R_a)**	**RMS Roughness (R_q)**
Silicon	27 nm	36 nm
FR4	506 nm	572 nm
FR4 with Copper	196 nm	260 nm

Using silicon as a substrate allows for a smooth surface to prevent roughness but may not be suitable for application where silicon has a low transmission coefficient for wireless signals. For such application FR4 is used which has considerably higher roughness. Using FR4 with a copper layer reduces the roughness of the layers to mitigate this problem seen in Table 6.2. This roughness additionally causes non-uniform thickness of layers; therefore, making the device more prone to dielectric breakdown. Future studies can further explore at this possibility to increase the electro-optic poling efficiency by decreasing this roughness caused from fabrication and design constraints.

6.2.5 Setup and Measurement

Alternatives in setup may improve the poling capabilities and measurement that are seen in this thesis. This includes different forms of poling, poling apparatus modifications, and alternative measurement methods for the electro-optic coefficient.

6.2.6 Corona Poling

Another poling method with potential is called Corona poling. This method consists of dangling a needle or matrix of needles above the top electrode with high voltage.

The voltage supply needs to be on the order of 5-10 kV [19, 56, 57]. The potential of the needle influences charge to gather on the top electrode and can be analogous to a capacitor gathering charge. The bottom electrode is grounded causing an electric field potential and chromophores to align. The advantage of this method is that charge will remain on the surface if there is an electrical short connection instead of causing damage and loss of the electric field from the stacked layer. Since the frequent occurrence of electrical shorts within thin films and imperfections that cause damage at relatively low voltages corona poling was considered. Corona poling could solve issues of electrical shorts, but it introduces non-uniformity in the electric field and therefore non-uniformity in poling [58]. The effect of the electric field uniformity can be tested by measuring the r_{33} at different locations after corona poling.

6.2.7 Poling Setup Upgrades

Currently, the apparatus for conducting electro-optic poling has room for improvements. A large issue is with the oven temperature consistency. The Hotpack from Figure 3.7 does not have the stability desired for efficient electro-optic poling. The interior capacity of the oven allows for large samples to be poled but causes local temperature variations. This makes it difficult to not exceed T_g and increases the possibility of dielectric breakdown. Use of a more stable oven for prolonged poling at T_g is also a common practice when poling. Keeping the sample near T_g with an

electric field present for an extended period of time may allow for more chromophores to align.

Because of the heat capacity of the poling oven it cannot be cooled quickly without opening the oven door or introducing liquid CO_2. A faster cool down period could be accomplished by using a smaller oven and using N_2 to blow over the sample [10, 39].

6.2.8 Measurement of Electro-Optic Coefficient (r_{33})

From Section 4.2.1 there is a change in refractive index of poled SEO100C compared to non-poled material. Future tests could examine at the linearity of the step increase of index of refraction as it relates to the electric field strength per μm.

The electro-optic coefficient of thin films can be measured using the Teng-Man method in Figure 2.4. This method is a standard for measuring the r_{33} of thin film materials and would be more beneficial than knowing the index of refraction step in Section 4.2. For measuring the electro-optic coefficient of devices such as a MZI the V_π is suitable.

References

[1] M. Balakrishnan, M. Faccini, M. B. J. Diemeer, E. J. Klein, G. Sengo, A. Driessen, W. Verboom, and D. N. Reinhoudt. Microring resonator based modulator made by direct photodefinition of an electro-optic polymer. *Applied Physics Letters*, 92(15):153310, 2008.

[2] Guofang Fan, Yuan Li, Bing Han, Qi Wang, Xinhou Liu, and Zhen Zhen. Study of an electro-optic polymer modulator. *Journal of Lightwave Technology*, 30(15): 2482–2487, August 2012.

[3] Zihang Zhu, Shanghong Zhao, Xuan Li, Kun Qu, Tao Lin, and Baoquin Lin. Dynamic range improvemnet for an analog photonic link using an integrated electro-optic dual-polarization modulator. *IEEE Photonics Jouranl*, 8(2), April 2016.

[4] G.L. Li and P.K.L. Yu. Optical intensity modulators for digital and analog applications. *Journal of Lightwave Technology*, 21(9):2010–2030, September 2003.

[5] Mark Lee, Howard E. Katz, Christoph Erben, Douglas M. Gill, Padma Gopalan, Joerg D. Heber, and David J. McGee. Broadband modulation of light by using an electro-optic polymer. *Science*, 298(5597):1401–1403, 2002.

[6] Oscar D. Herrera. *Nonlinear Photonics in Waveguides for Telecommunications*. PhD thesis, The University of Arizona, November 2014.

[7] Lumera. Applications of electro-optic polymers and devices: Breaking the high frequency, broad bandwidth barrier. Lumera Corporation, February 2008.

[8] Roland Himmelhuber, Robert A. Norwood, Yasufumi Enami, and Nasser Peyghambarian. Sol-gel material-enabled electro-optic polymer modulators. In *Sensors*, 2015.

[9] G.K. Gopalakrishnan, C.H. Bulmer, W.K. Burns, R.W. McElhanon, and A.S. Greenblatt. 40 ghz low half-wave voltage ti:linbo$_3$ intensity modulator. *Electronic Letters*, 28(9):826–827, April 1992.

[10] David L. K. Eng, Stephen Kozacik, Shouyuan Shi, Benjamin C. Olbricht, and Dennis W. Prather. All-polymer modulator for high frequency low drive voltage applications. In Christopher E. Tabor, Francois Kajzar, Toshikuni Kaino, and Yasuhiro Koike, editors, *Organic Photonic Materials and Devices*, volume 8983, pages 898316–898316–8. SPIE, March 2014.

[11] Tsvi Katchalski, Guy Levy-Yurista, Asher A. Friesem, Guillermo Martin, Rolland Hierle, and Joe Zyss. Light modulation with electro-optic polymer-based resonant grating waveguide structures. *Opt. Express*, 13:4645–4650, June 2005.

[12] Xiaojun Xie, Kejia Li, Qiugui Zhou, Andreas Beling, and Joe C. Campbell. High-gain, low-noise-figure, and high-linearity analog photonic link based on a high-performance photodetector. *Journal of Lightwave Technology*, 32(21):3585–3590, November 2014.

[13] Yongqiang Shi, Weiping Lin, David J. Olson, James H. Bechtel, Hua Zhang, William H. Steier, Cheng Zhang, and Larry R. Dalton. Electro-optic polymer modulators with 0.8 v half-wave voltage. *Applied Physics Letters*, 77(1):1–3, 2000.

[14] Hui Hu, Fei Lu, Xue Lin Wang, Feng Chen, and Ke Ming Wang. Low-loss optical waveguides and y-branch splitters in lithium niobate fabricated by mev oxygen ions with low dose. *Optics Express*, 20(19):21114–21118, September 2012.

[15] E. L. Wooten, K. M. Kissa, A. Yi-Yan, E. J. Murphy, D. A. Lafaw, P. F. Hallemeier, D. Maack, D. V. Attanasio, D. J. Fritz, G. J. McBrien, and D. E. Bossi. A review of lithium niobate modulators for fiber-optic communications systems. *IEEE Journal of Selected Topics in Quantum Electronics*, 6(1):69–82, January 2000.

[16] David L. K. Eng, Stephen T. Kozacik, Ilya V. Kosilkin, John P. Wilson, Dylan D. Ross, Shouyuan Shi, Larry Dalton, Benjamin C. Olbricht, and Dennis W. Prather. Simple fabrication and processing of an all-polymer electrooptic modulator. *IEEE Journal of Selected Topics in Quantum Electronics*, 19:3401306, 2013.

[17] Datong Chen, Harold R. Fetterman, Antao Chen, William H. Steier, Larry R. Dalton, Wenshen Wang, and Yongqiang Shi. Demonstration of 110 ghz electro-optic polymer modulators. *Applied Physics Letters*, 70(25):3335–3337, 1997.

[18] Jingdong Lou. *Soluxra Processing Description of SEO100C*. Soluxra, LLC, PO Box 85285, Seattle, WA 98145, USA, June 2015.

[19] Edward M. McKenna, Andy S. Lin, Alan R. Mickelson, Raluca Dinu, and Dan Jin. Comparison of r33 values for aj404 films prepared with parallel plate and corona poling. *Journal of the Optical Society of America*, 24(11):2888–2892, November 2007.

[20] Y. Jouane, Y-C. Chang, D. Zhang, J. Luo, A. K-Y. Jen, and Y. Enami. Unprecedented highest electro-optic coefficient of 226 pm/v for electro-optic polymer/-tio2 multilayer slot waveguide modulators. *Opt. Express*, 22(22):27725–27732, November 2014.

[21] Roberto S. Aga, Jr., Fahima Ouchen, Alyssa Lesko, Brian A. Telek, Emily M. Fehrman Cory, Carrie M. Bartsch, Jack Lombardi, III, James Grote, and

Emily M. Heckman. Polymeric waveguide electro-optic beam-steering device with dna biopolymer conductive cladding layers. *Optical Engineering*, 51(11): 114602, 2012.

[22] Tae-Dong Kim, Jingdong Luo, Yen-Ju Cheng, Zhengwei Shi, Steven Hau, Sei-Hum Jang, Xing-Hua Zhou, Yanqing Tian, Brent Polishak, Su Huang, Hong Ma, Larry R. Dalton, and Alex K.-Y. Jen. Binary chromophore systems in nonlinear optical dendrimers and polymers for large electrooptic activities. *The Journal of Physical Chemistry C*, 112(21):8091–8098, 2008.

[23] Hiroshi Nishihara, Masamitsu Haruna, and Toshiaki Suhara. *Optical Integrated Circuits*. McGraw Hill, 1985.

[24] Xiaoqiang Sun, Ying Xie, Xuliang Zhao, Dehui Li, Shimin Zhao, Yuanbin Yue, Xibin Wang, Jian Sun, Lei Liang, Changming Chen, Daming Zhang, Fei Wang, and Zhiyuan Xie. Effect of film compatibility on electro-optic properties of dye doped polymer dr1/su-8. *Applied Surface Science*, (285):469–476, November 2013.

[25] Charles H. Cox III and Edward I. Ackerman. High electro-optic sensitivity (r33) polymers: They are not just for low voltage modulators any more. *Journal of Physical Chemistry*, 108(25):8540–8542, 2004.

[26] S. Herminghaus, Barton A. Smith, and J. D. Swalen. Electro-optic coefficients

in electric-field-poled polymer waveguides. *J. Opt. Soc. Am. B*, 8(11):2311–2317, November 1991.

[27] Stefan Prorok, Alexander Petrov, Manfred Eich, Jingdong Luo, and Alex K.-Y. Jen. Modification of a teng-man technique to measure both r33 and r13 electro-optic coefficients. *Applied Physics Letters*, 105(11):113302, 2014.

[28] Dong Hun Park, Chi H. Lee, and Warren N. Herman. Accuracy of the atr method for electro-optic measurement of poled polymer thin films in multilayer structures. In *Frontiers in Optics 2007/Laser Science XXIII/Organic Materials and Devices for Displays and Energy Conversion*, page JWC52. Optical Society of America, 2007.

[29] Dong Hun Park, Jingdong Luo, Alex K.-Y. Jen, and Warren N. Herman. Simplified reflection fabry-perot method for determination of electro-optic coefficients of poled polymer thin films. *Polymers*, 3(3):1310–1324, 2011.

[30] R. Ulrich and R. Torge. Measurement of thin fil parameters with a prism coupler. *Applied Optics*, 12(12):2901–2908, December 1973.

[31] P. K. Tien and R. Ulrich. Theory of prism–film coupler and thin-film light guides. *J. Opt. Soc. Am.*, 60(10):1325–1337, October 1970.

[32] P. K. Tien. Light waves in thin films and integrated optics. *Applied Optics*, 10 (11):2395–2413, November 1971.

[33] J. H. Harris, R. Shubert, and J. N. Polky. Beam coupling to films. *J. Opt. Soc. Am.*, 60(8):1007–1016, August 1970.

[34] C. C. Teng and H. T. Man. Simple reflection technique for measuring the electro-optic coefficient of poled polymers. *Applied Physics Letters*, 56(18), 1990.

[35] Arnaud Gardelein, Sylvain Le Tacon, Eric Tanguy, Nicolas Breuil, and Tchanguiz Razban. Characterization of electrooptic polymer applied to microwave sensing. *Microwave Photonics*, 2006.

[36] Yuuki Kashiyama, Jionghao He, Shinjiro Machida, and Kazuyuki Horie. Large photoinduced refractive index change in a polyimide film by charge-transfer complex formation with a polymer-bound phenylazide fragment. *Macromolecular Rapid Communications*, 22(3):185–188, 2001.

[37] Huajun Tang, John M. Taboada, Guohua Cao, Liqiang Li, and Ray T. Chen. Enhanced electro-optic coefficient of nonlinear optical polymer using liquid contact poling. *Applied Physics Letters*, 70(5):538–540, February 1997.

[38] Robert C. Hoffman, Andrew G. Mott, Michael J. Ferry, Timothy M. Pritchett, William Shensky III, Joshua A. Orlicki, George R. Martin, Joseph Dougherty, Julia L. Leadore, Adam M. Rawlett, and Dong Hun Park. Poling of visible chromophores in millimeter thick pmma host. *Optical Materials Express*, 2011.

[39] Emily Marie Fehrman Cory. *Fabrication of a deoxyribonucleic acid polymer ridge*

waveguide electro-optic modulator by nanoimprint lithography. PhD thesis, University of Dayton, 2014.

[40] Perry P. Yaney, Emily M. Heckman, and James G. Grote. Resistivity and electric-field poling behaviors of dna-based polymers compared to selected non-dna polymers. In Emily M. Heckman, Thokchom B. Singh, and Junichi Yoshida, editors, *Nanobiotronics*, volume 6646, pages 664605–664605–10. SPIE, SPIE Proceedings, September 2007.

[41] Perry P. Yaney, Emily M. Heckman, Antonio Davis, Joshua A. Hagen, Carrie M. Bartsch, Guru Subramanyam, James G. Grote, and F. Kennenth Hopkins. Characterization of nlo polymer materials for optical waveguide structures. In James G. Grote, Francois Kajzar, and Nakjoog Kim, editors, *Organic Photonic Materials and Devices VIII*, volume 6117, February 2006.

[42] Emily M. Heckman, Carrie M. Bartsch, Adam T. Rossbach, Brian A. Telek, and James G. Grote. Poling and characterization studies in electro-optical polymers with dna cladding layers. In *Nanobiosystems: Processing, Characterization, and Applications III*, volume 7765, page 776505, August 2010.

[43] Sebastien Michael, Joseph Zyss, Isabelle Ledoux-Rak, and Chi Thanh Nguyen. High-performance electro-optic modulators realized with a commercial side-chain dr1-pmma electro-optic copolymer. In Robert L. Nelson, Francois Kajzar, and

Toshikuni Kaino, editors, *Organic Photonic Materials and Devices XII, Proceedings of SPIE*, volume 7599, page 759901. SPIE, March 2010.

[44] Jingdong Lou. *Soluxra Processing Description of SEO125B*. Soluxra, LLC, PO Box 85285, Seattle, WA 98145, USA, December 2015.

[45] Emily M. Heckman, James G. Grote, F. Kenneth Hopkins, and Perry P. Yaney. Performance of an electro-optic waveguide modulator fabricated using a deoxyribonucleic-acid-based biopolymer. *Applied Physics Letters*, 89(18):181116, 2006.

[46] Reem Song, Hyunchae Song, and William H. Steier. Novel mach-zehnder polymer modulators using coplanar waveguide electrodes. In *Frontiers in Optics*, page SWA2. Optical Society of America, 2005.

[47] Hadi Baghshiahi, Kai Wang, Witold Kandulski, Richard Charles A.Pitwon, and David R. Selviah. Optical waveguide end facet roughness and optical coupling loss. *Jouranl of Lightwave Technology*, 31(16):2659–2668, August 2013.

[48] Grover L. Larkins. Thin film multilayer high tc superconductor structures. Technical report, Florida International University, Electrical Engineering Department, Florida International University, Miami, Florida 33199, February 1997.

[49] Keith Barkley. *Two-Tone IMD Measurement Techniques*. RF Design, June 2001.

[50] *Spurious Free Dynamic Range*. Fiber Span, 3434 Route 22W Branchburg, New Jersey 08876.

[51] Agilent. Two-tone and multitone personalities for the e8267c psg vector signal generator. Technical report, Agilent Technologies, Inc., February 2013.

[52] T. G. Nguyen, Y. S. Visagathilagar, and A. Mitchell. Rf-photonic link using a resonantly-enhanced mach-zehnder optical modulator. In *2005 International Topical Meeting on Microwave Photonics*, pages 253–256, October 2005.

[53] Brian H. Kolner and David W. Dolfi. Intermodulation distortion and compression in an integrated electrooptic modulator. *Applied Optics*, 26(17):3676–3680, September 1987.

[54] Anthony Holland, Patrick Leech, and G. K. Reeves. Reactive ion etching of organic polymers for application in waveguide trench molds. *Journal of Materials Science*, 39(10):3505–3508, May 2004.

[55] Fahima Ouchen, Emily Heckman, Larry Dalton, Francois Kajzar, Ileana Rau, and James Grote. Effect of charge carrier blocking surface resistance and electric field distribution on electric field poling of nonlinear optic polymers. In Christopher E. Tabor, Francois Kajzar, Toshikuni Kaino, and Yasuhiro Koike, editors, *Organic Photonic Materials and Devices XIX*, volume 10101, 2017.

[56] Charles Lee, William Steier, Lary Dalton, and Harold Fetterman. Electro-optical

polymer technology. Technical report, AFOSR and University of Southern California and University of California, 1999.

[57] Xavier Borg. Blaze labs ehd thrusters research home of the highest performance ehd thruster cells. www.blazelabs.com/l-intro.asp, 2017.

[58] J. A. Giacometti and O. N. Oliveira. Corona charging of polymers. *IEEE Transactions on Electrical Insulation*, 27(5):924–943, October 1992.

Appendix A

Resistivity Data

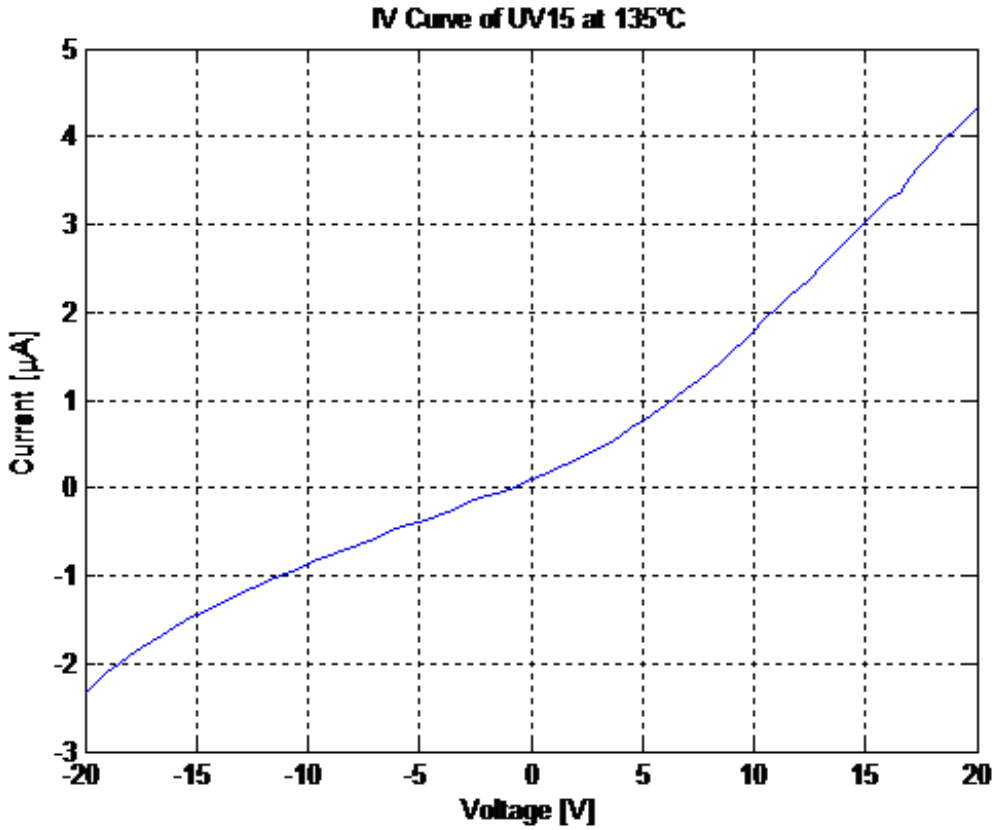

Figure A.1: Current versus voltage curve of resistivity measurements

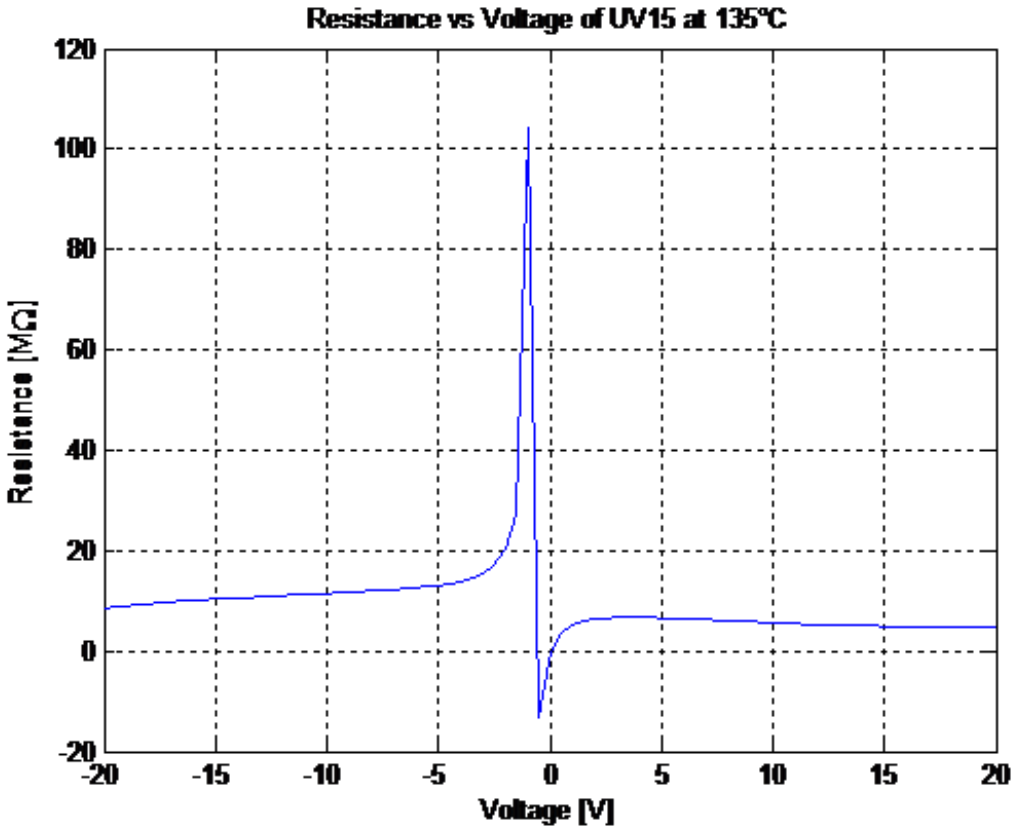

Figure A.2: Resistance versus voltage curve of resistivity measurements

Appendix B

Electro-Optic Poling Data

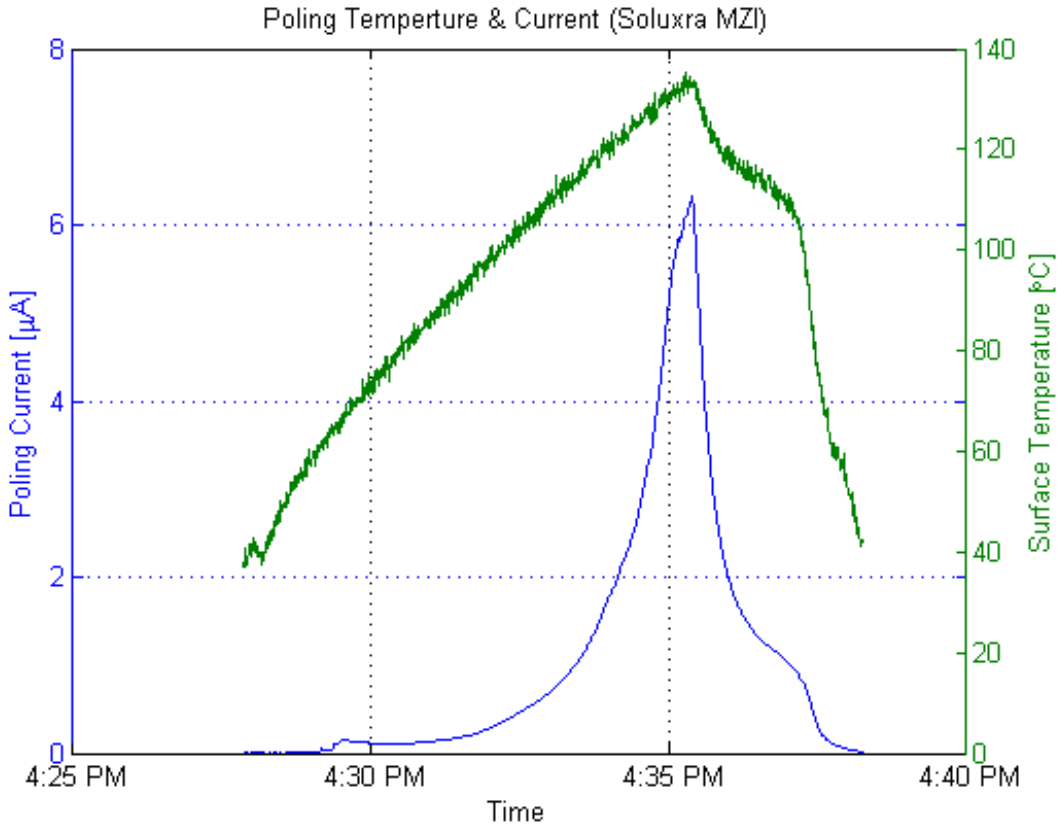

Figure B.1: Data collected from poling of a Mach-Zehnder at 350 V

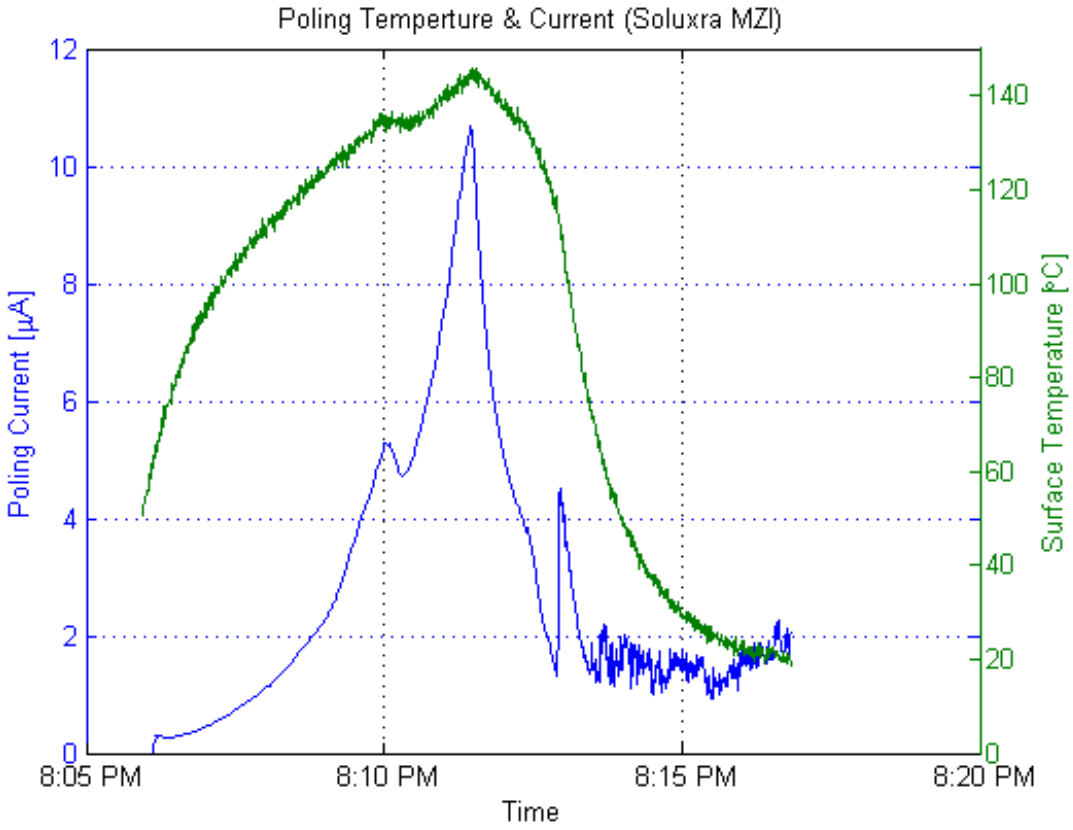

Figure B.2: Data collected from poling of a Mach-Zehnder at 430 V

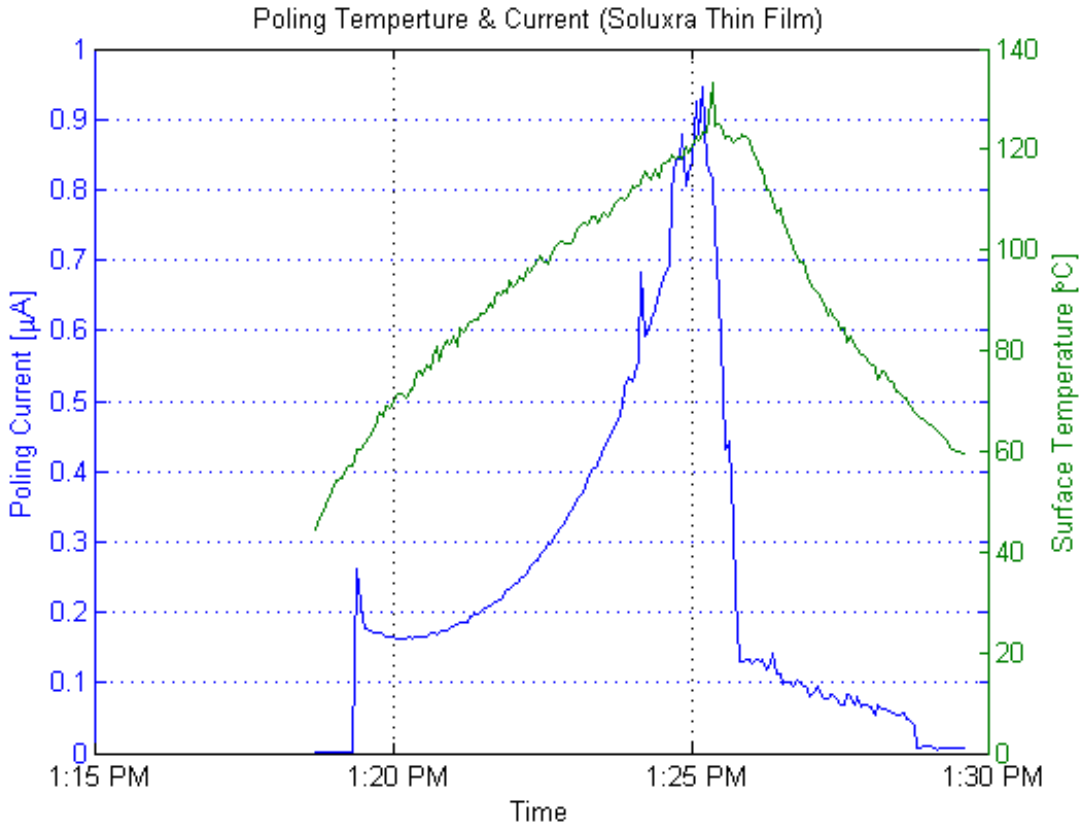

Figure B.3: Data collected from poling of a thin film at 100 V

Appendix C

Letters of Permission

AIP PUBLISHING LLC LICENSE TERMS AND CONDITIONS

Mar 29, 2017

This Agreement between Michael Briseno ("You") and AIP Publishing LLC ("AIP Publishing LLC") consists of your license details and the terms and conditions provided by AIP Publishing LLC and Copyright Clearance Center.

License Number	4078010666473
License date	Mar 29, 2017
Licensed Content Publisher	AIP Publishing LLC
Licensed Content Publication	Applied Physics Letters
Licensed Content Title	Simple reflection technique for measuring the electro-optic coefficient of poled polymers
Licensed Content Author	C. C. Teng, H. T. Man
Licensed Content Date	Apr 30, 1990
Licensed Content Volume	56
Licensed Content Issue	18
Type of Use	Thesis/Dissertation
Requestor type	Student
Format	Electronic
Portion	Figure/Table
Number of figures/tables	1
Title of your thesis / dissertation	Electro-Optic Contact Poling of Polymer Waveguide Devices and Thin Films
Expected completion date	May 2017
Estimated size (number of pages)	120
Requestor Location	Michael Briseno 906 Jasper Ave. HOUGHTON, MI 49931 United States Attn: Michael Briseno
Billing Type	Invoice
Billing Address	Michael Briseno 906 Jasper Ave. HOUGHTON, MI 49931 United States Attn: Michael Briseno
Total	0.00 USD
Terms and Conditions	

AIP Publishing LLC -- Terms and Conditions: Permissions Uses

Figure C.1: Letter of Permission for Figure 4.1